Reservoir Simulation of Hoobler Study Area – Chase/Council Grove Reservoir Systems

Kansas Geological Survey

Open File Report No. – 2006-27

Authors:

Saibal Bhattacharya

Martin K. Dubois

Alan P. Byrnes

1.0 Introduction

The Hugoton and Panoma gas fields (Figure 1), North America's largest, produce from 13 fourth-order marine-nonmarine sedimentary cycles of the Wolfcampian Chase and Council Grove Groups, respectively. A fine-layered cellular geomodel was constructed for these fields using a four step workflow: 1) define lithofacies in core and correlate to wireline log curves and geologic variables (depositional environment and relative cycle-position), 2) train a neural network and predict lithofacies at non-cored wells, 3) populate a 3D cellular model with lithofacies using stochastic methods, and 4) populate the model with petrophysical properties and fluid saturations using facies-specific equations based on core data. The fine-scale model was upscaled to 25 layers for simulation.

2.0 Objective

The objective of this study was to validate the above mentioned geomodel by simulating the production/pressure performance of wells located in select multi-section areas in the Hugoton field. The reservoir geomodel was developed using an automated facies-recognition technique and specific capillary pressure curves developed by integrating available core data. The intent of this exercise is, therefore, to evaluate the robustness of this geomodel by comparing how close the simulator-calculated pressure/production performances of individual wells match with respective histories with minimum modifications to the geomodel. The focus is not to obtain exact matches of pressure/production histories at individual wells with localized model modifications. Computer Modeling Group's (CMG's) IMEX simulator was used in this study.

This report details the simulation studies carried out at one such area – 12 sections around the Hoobler Estate Unit well (Section 20, Township 6N, Range 17E). The location of the Hoobler simulation area within the context of the Hugoton-Panoma fields is shown in Figure 1 while Figure 2 shows the locations of the wells within this study area.

Some of the reasons behind selection of this study area include: a) location outside the Panoma field and on the edge of the "other" Council Grove production area, b) presence of relatively thick Chase gas column, c) availability of Chase core from within the study area and nearby Council Grove cores, and d) presence of limited layer pressure data from 1995 and 2005. Figure 3 shows that 6 node wells with modern log suite and three wells with zone pressure data are present within the Hoobler study area. Figure 4 shows the position of wells in and around the study area where RFT layer-pressures were available.

3.0 Model Inputs

3.1 Hoobler area geologic model

The Hoobler area is located in the east central portion of the Hugoton field on the Oklahoma side of the Kansas-Oklahoma border. The model is situated immediately shelfward of an area of steepened dip on the Wolfcamp ramp (or gently dipping shlf, that has been interpreted as a shelf margin (Dubois, et al., 2006). The Hoobler study area is outside the Panoma field and the Coucnil Grove production on the east side of the study area is from a closed structural feature that is downdip from and unrelated to the Panoma gas filed accumulation. Here the Chase and Council Grove reservoirs behave as separate gas reservoirs and the Council Grove was not simulated.

3.2 Static model

The nine-section Hoobler static model was extracted from the field-wide geomodel version Geomod (Figure 5) and upscaled from 269 layers to 24 layers for the simulation model (Figure 6). Figure 5 shows the area extracted from the larger model. The xy grid dimensions are 660 feet by 660 feet (200 m by 200 m). Since the model is outside the Panoma and layers within the model below layer 11 are 100% water saturated, the model was reduced to the top 11 zones, the Chase through the Council Grove A1_SH. In reality the Council Grove does not have 100% water saturation in the

closed structure on the east side of the model. Our current geomodel is focused only on the Panoma that has a much higher (structurally) free water level (FWL). Figure 7 shows the distribution of GIP for the eleven-layer model with a FWL at +65 feet above sea level and Figure 8 illustrates the other critical properties. Corrected porosities at the node wells were estimated using algorithms developed from core to log porosity regression analysis (Figure 9).

3.3 Engineering Model

The 11-layer geomodel was exported to the reservoir simulator – Computer Modeling Group's IMEX. Each layer in this 11-layer model coincided with a formation- or member-level stratigraphic interval in the Chase system. Each layer represents a half-cycle of marine/non-marine sedimentary cycle. In most cases, the model layer closely approximates the RFT intervals at wells in and around the study area. The area simulated extends over 12 sections around the Hoobler Estate Unit well. Grid cell dimensions were set at 660 ft by 660 ft for all layers.

Porosity was upscaled using an arithmetic average, conditioned on lithofacies; water saturation was upscaled using a porosity weighted arithmetic average, and permeability was upscaled utilizing flow-based tensor upscaling using PSK-solver.

Figure 10 lists the basic PVT properties input for simulation.

3.4 Permeability Modeling

Porosity-permeability measurements taken on whole cores on a foot-by-foot basis were available from the Chase interval at Hoobler EU well. Permeability recordings from Krider, Winfield, and Towanda zones at the above mentioned wells are shown in Figure 11. Permeability was not measured on core-plugs from the available core.

Fundamental to modeling the permeability distribution in the Hugoton is the need to understand the relative role of matrix and fracture flow and the possible scale dependence of permeability. Figure 12 displays measured permeability-porosity data from fractured whole cores, unfractured whole cores, and unfractured core plugs from other available cores from the Hugoton study. Whole-core (full-diameter) values diverge from matrix (plug) values at porosities less than ~10%. This can be interpreted to indicate the dominant influence of microfracture(s) on permeability in whole-core samples with porosity < 10% and corresponding permeability < ~0.5 md. Above 10 % porosity influence of microfracure(s) is small, and the whole core and core plug values overlap.

A question that naturally arises from these data is: are the microfractures present in the subsurface or are they a stress release or coring-induced phenomenon? This question can only be answered by comparing upscaled matrix permeabilities with unfractured full-diameter permeabilities and with drill stem test (DST) or well-test calculated permeabilities. Figure 13 crossplots full-diameter core porosity versus plug porosity (A) and plug permeability versus full-diameter permeability (B) for samples in which the full-diameter cores did not exhibit any apparent microfracturing. Good correlation in both the above plots indicates that matrix-scale properties apply to full-diameter scale. Variance can be attributed to full-diameter core sampling multiple lithofaceis or a range in porosity not sampled by the corresponding core plug.

The ability to compare well-scale permeability with matrix permeability is limited because so few wells have DST or well test data recorded prior to hydraulic fracturing and over specific intervals for which core data are available. In four key research wells, permeability was measured with DSTs across specific intervals where core analysis was also performed. To compare with core permeabilities, full-diameter and plug permeabilities were arithmetically averaged (representing parallel flow contribution from each depth interval) to determine average interval permeabilities. Correlation between DST permeability and upscaled full-diameter and plug permeabilities shows good correlation (Figure 14) for intervals with permeability greater than ~0.5 md (0.0005 μm^2). For interval permeabilities below 0.5 (0.0005 μm^2) md, full-diameter permeabilities

exhibit nearly constant permeability between 0.5 and 3 md (0.0005-0.000033 μm^2), characteristic of microfracture-influenced permeability. Matrix-scale plug permeabilities are both higher and lower than DST permeabilities (Figure 14).

As mentioned earlier, whole-core permeabilities were measured on a foot-by-foot basis from the Chase core retrieved from the Hoobler EU well. The whole-core derived (horizontal) permeability values were arithmetically averaged (upscaled) to derive the layer horizontal permeability. Absent layer-DST permeability values, the upscaled layer permeability derived from whole cores was assumed to be representative of effective permeabilities in each layer within the drainage area of the Hoobler EU well.

The geomodel built in Petrel® consisted of 269 layers. Facies-specific permeability-porosity co-relationships were used to estimate of grid permeabilities from grid porosities. The tensor upscaling algorithm in Petrel® was used to upscale vertical and horizontal permeability to 11 layers before exporting the model to CMG. For each layer at the place of location of the Hoobler EU well, the upscaled permeability (from Petrel®) was compared with that calculated by upscaling the whole-core-based permeability values (Figure 15). For layers where the upscaled permeability differed from whole-core permeability, an appropriate multiplier was applied so that the layer permeability matched that calculated by upscaling whole-core measurements. For each layer, Figure 15 tabulates the multiplier applied so that the grid cell permeability at the location of the Hoobler EU well in the CMG model matched the corresponding upscaled whole-core layer-permeability. As discussed in the previous section, whole-core K values are higher than plug K below 0.5 md because micro-fractures present in whole cores result in measured K values to exceed 0.5 md. Also, plugs are biased to represent matrix rock and possible are minimally affected by micro-fractures especially in tight rocks. Thus, multipliers close to 1.0 were found applicable for pay layers where average whole-core K values are higher than 0.5 md.

3.5 Natural Fractures

Variance between DST- and core-plug-permeabilities are partially or predominantly related to the limited vertical sampling of the core plugs and difficulty in representing some pore properties that are larger in scale than core plugs. The single phylloid algal bafflestone interval exhibits significantly lower matrix permeability because core plugs did not sample the larger-scale vuggy nature of this lithofacies, which exhibits high permeability. Since microfractures do not contribute significantly to measured permeability for rocks with permeability greater than 0.5 md (0.0005 μm^2), both full-diameter and plug data reflect matrix properties and the good correlation with DST permeabilities. This indicates that the reservoir is not fractured at the scale of investigation of the DST test. The better correlation of plug and DST permeabilities for intervals with permeability below 0.5 md, and the fact that upscaled permeabilities from plug data are greater than or equal to DST permeabilities, for three of the four intervals, can be interpreted to indicate that these intervals are also unfractured. These data, and less precise data from other wells, indicate that the production characteristics of many wells in the Hugoton are consistent with matrix properties without significant natural fracture contribution.

3.6 Reservoir Pressure

The first recorded surface shut-in (SI) pressures (soon after completion) at the Chase Parent wells in the area studied varied between 390 to 423 psi (Figure 16). Surface shut-in pressures were converted to bottom-hole shut-in pressures. Figure 17 shows the estimation of initial reservoir pressure from recorded surface shut-in pressures following the average temperature and z-factor method. The estimated initial reservoir pressure was about 450 psi assuming a WHSP of 420 psi. Thus, the reservoir model in the simulator was initialized using a starting pressure of 450 psi, and resulted in charging the input geomodel (for the area studied) with an original-gas-in-place (OGIP) of 131.1 bcf (as compared to 128 bcf in the Petrel geomodel, Figure 18).

3.7 Hydraulic Fractures

Most of the wells in the study area were drilled before 1950. Current records indicate that all wells were hydraulically fractured some time during their production life. However, the exact date on which each well was fractured is not available. Fracturing technology came in use in the study area some time in the early 1970s. In this study, it was assumed that wells were fractured as of January 1, 1970. Later infill/replacement wells drilled in the 1980s or later were assumed to be fractured upon completion.

However, there is no information or test data available which would enable one to estimate the physical characterization of these fractures. The intent of the fracturing was to enhance the well productivity. Lacking physical descriptions of hydraulic fractures, the enhanced well productivities were modeled in this study using the well productivity (ff) factor greater than 1 with the ff set to 1.0 for an un-fractured well. The ff value was modified at each well to match the post-1970 production.

3.8 Flow Constraints

Annual production data for individual wells were available for initial completion to 1966. From 1967 onwards, monthly production data were available for all the Chase wells in the study area. Regular tubing head flow and shut-in pressure data were available for all wells from 1967 onwards.

In the simulator, all wells were flowed under rate constraints until April 2005. Thereafter, all wells were flowed under a constant bottom-hole pressure (BHP) of 14.7 psi till May 2006. The intent of changing from rate constraint to pressure constraints was to see if the simulator-calculated production rates from May 2005 to May 2006 followed the already established decline trends without showing production spikes (or signs of excess flow capacity). The well names and their abbreviated names used in the simulator model along with their starting dates, cumulative production, and initial perforation intervals are listed in Figure 19.

4.0 Reservoir Simulation Studies

The completion records (Figure 20) indicate that the Chase wells were initially perforated in the upper four layers, i.e., Herrington, Krider, Odell, and Winfield. Well operators confirm that each of these wells was hydraulically fractured during some point in its production life. However, the exact date when each well was fractured is unavailable. In the model, it was assumed that each well was fractured as of January 1, 1970 – the approximate time frame when fracturing came in vogue in the study area. Figure 4 reveals that the Chase wells in the study area produced around 70.13 bcf while the OGIP charged in the first 4 layers totals 58 bcf. Thus to obtain a match with production history, gas from lower layers such as the Towanda and the Fort Riley has to be produced. If the completion is assumed to be restrained to L4 (Winfield), then the gas from the lower layers has to flow across the intervening shale zones taking advantage of vertical permeabilities.

The model used in this study was an 11-layer model with grid cell sizes of 660 feet by 660 feet. A consistent set of legends was used to analyze the simulation results. The simulator-calculated production and bottom-hole flowing pressure are displayed in red and green lines while the historic production and well head flowing pressures (WHFPs) are displayed in blue and magenta.

Because the wells were not fractured pre-1970, flow in this period was dominated by matrix. Also during this period, the well completions did not extend beyond the perforated layers. Thus, the strategy employed in the designing the following set of simulation runs was to first try to match pre-1970 field production by adjusting matrix permeability through the application of different multipliers. After obtaining a match with the historic production volumes prior to January 1 1970, other factors such as layers drained by the fractures and productivity gains from hydraulic fracturing were modified on a well-by-well basis to improve both the production and flowing pressure matches at each well.

4.1 RUN 1

All wells were initially completed as per available information from well records (Figure 20). Wells without any initial completion records were assumed to be completed in the upper four layers. As of January 1, 1970, all wells were fractured in the simulator using an ff = 6.0. However, the fractures were constrained to the initial completion interval at each well. Also, (horizontal) permeability multipliers (Figure 15) were applied to layers 1, 2, and 4 only, i.e. L1, L2, and L4. As a result of the application of these multipliers, the layer permeability in each of the above mentioned layers around the Hoobler EU well in the simulator model corresponds closely to the whole-core based upscaled permeability. Permeability multipliers were not applied to the shale layers such as L3 (Odell). Results from this run are shown in Figures 21. The simulator-calculated production falls short by about 8 bcf before 1970 and by about 20 bcf in 2005.

Figures 22 and 23 display the production and pressure matches obtained at individual wells. The simulator-calculated production (red line) falls short of history (blue line) for many wells even before 1970. Thus, matrix K appears insufficient to match pre-1970 production at most wells. However, simulator-calculated production matched history at Wilson (named Wils in simulation results) and Blackmer 28 (named Blk28 in simulation results). Figure 24 shows that there is a bull's eye in the horizontal permeability distribution in Winfield (Layer 4) around Blk28 as it is significantly higher than in other parts of the study area. It appears that the automated facies-prediction model must have incorrectly assigned facies in this area and, therefore, resulted in non-representative permeability estimations. Also, the simulator-calculated bottom-hole flowing pressure (BHFP, in green line) is consistently higher than the historically recorded WHFP (in magenta) indicating excess gas and/or flow capacity in the drainage area of Blk28. As for Wilson (named Wils in simulation results) the simulator-calculated BHFP is close to the historic WHFP. However, the simulator-calculated production falls short of the historic production near the year 2000.

RFT records from wells in and around the study area were available. Despite variations between readings from within a layer, reservoir pressures in Krider (L2) and Winfield (L4), as of 2005, were estimated to be between 40 to 60 psi respectively. Figure 25 lists the best estimates of layer pressures in the study area as of 2005. Figure 26 shows the pressure distribution through an east-west cross section across the Hoobler EU well as of May 2006. These simulator-calculated results indicate that the pressure in Krider (L2) varies between 50 to 130 psi while that in Winfield (L4) varies between 90 to 300 psi.

4.2 RUN 2

The horizontal permeability (Kxy) distribution in L2 (Krider) was multiplied by 2 (over the starting multiplier) in order to increase simulator-calculated gas production in the pre-1970 period. Figure 27 compares the simulator-calculated field production with historic volumes, and it becomes evident that as of 1970, the simulator-calculated cumulative production falls short by 5 bcf as opposed to 8 bcf in Run 1. Thus, additional gas needs to be mobilized in the pre-1970 period in the simulator model. A display of pressure distribution (Figure 28) in an east-west cross-section through the Hoobler EU (HobEU) wells shows that the pressure in Krider (L2) layer is less than 85 psi while that at HobEU is 39 psi. Thus, L2 appears to have drained close to best estimates from RFT data, i.e., layer pressure varying between 40-60 psi.

4.3 RUN 3

The horizontal permeability (Kxy) distribution in L4 (Krider) was multiplied by 2 (over the starting multiplier) in order to increase simulator-calculated gas production in the pre-1970 period. Thus, both L2 and L4 have a multiplier of 2 applied on the permeability distribution present in Run 1. Figure 29 compares the simulator-calculated field production with historic volumes, and it becomes evident that as of 1970, the simulator-calculated cumulative production falls short by 2 bcf as opposed to 5 bcf in Run 2. Hence, additional gas still needs to be mobilized in the pre-1970 period in the simulator model. A display of pressure distribution (Figure 30) in an east-west cross-

section through the Hoobler EU (HobEU) wells shows that the pressure in Winfield (L4) layer is less than 260 psi while that at HobEU is 72 psi. Thus, L4 in the vicinity of the HobEU appears to have drained close to best estimates from RFT data, i.e., layer pressure varying between 40-60 psi.

4.4 RUN 4

To increase production from the simulator model, the Kxy distribution in L2 and L4 was multiplied by 3 over the initial multiplier, i.e., the permeability distribution in these layers in Run 1. Figure 31 compares the simulator-calculated field production with historic volumes. As of 1970, the simulator-calculated cumulative production still falls short of historic volumes by 0.92 bcf. Figure 32 shows the gas in place in Herrington (L1). As of 1970, there is about 3.25 bcf of gas in L1. Figure 33 shows the layer pressure distribution across a cross section through HobEU well. The pressure at HobEU is 70 psi while higher pressures prevail in L1 away from the well. As a comparison, the pressure at HobEU in L2 (Krider) is 33 psi while pressures away from the well in L2 never exceed 85 psi. Similarly, the pressure at HobEU in L4 (Winfield) is 62 psi while pressures away from the well in L4 never exceed 230 psi.

4.5 RUN 5

Figure 11 and Figure 34 tabulate the whole-core measured permeability distributions at HobEU well for Krider (L2), Winfield (L4), Towanda (L6), and Herrington (L1) respectively. The whole-core-based permeability values were upscaled in each of these layers and compared with that estimated from facies-specific permeability-porosity equations. Differences were reconciled using appropriate multipliers (Figure 15). These multipliers were used in the initial simulation run (Run 1) for L1, L2, and L4. A closer look at the whole-core data from these 3 layers reveals that there are streaks of high permeability in each of these layers. These high permeability zones are the drivers for gas production and yet get smoothed in the process of permeability upscaling (of the whole-core data). Permeability calculated from reservoir-pressure testing is considered most

representative to simulate well performance as it is the effective permeability prevalent in the drainage area of the well(s). Thus absent permeability calculated from well tests, layer permeability multipliers were calculated using the upscaled whole-core based permeability data, which under-represents the high permeability streaks. For example in Krider (Figure 11), the upscaled whole-core based permeability data is 2.24 md while the whole-core data reveal high streaks ranging between 3 to 6 md. It is impossible to estimate the effective permeability prevalent L2 (Krider) in the drainage area of HobEU well without a well test but critical examination of whole-core data indicates that application of permeability multipliers between 2 to 4 times the upscaled whole-core data is not unreasonable, especially when lower permeability distributions are unable to produce historically recorded gas volumes. Similar high permeability streaks are visible in the whole-core data in Herrington and Winfield.

Figure 35 shows the simulator-calculated production when the permeability distribution in L1, L2, and L4 were multiplied by 3 (over the initial distribution in Run 1). It appears that the simulator-calculated pre-1970 production is very close to historic volumes but still less by 0.92 bcf (as of 1970).

4.6 RUN 6

Figure 36 compares the simulator-calculated production with field history when the permeability distribution in L1, L2, and L4 were multiplied by 3 and that of L6 by 2 over the initial respective values in Run 1. The simulator-calculated production almost matches historic volumes as of 1970. Thus, even increasing permeability in L6 (Towanda) did not enable production history matching as of 1970.

4.7 RUN 7

Figure 37 compares the simulator-calculated production with field history when the permeability distribution in L1, L2, and L4 were multiplied by 4 over the initial respective values in Run 1. It is evident from Figure 4.7 that the simulator-calculated

production almost matched historic production volumes as of 1970. Thus given the geomodel (with its distribution of gas saturation), the matrix permeability distribution in L1, L2, and L4 had to be increased 4 times over that obtained by upscaling whole-core permeabilities at HobEU well in order to match historic pre-1970 production. Figures 38 and 39 display in the production/pressure matches obtained at individual wells. It appears that the simulator-calculated production matched pre-1970 historic production in all wells except Muller (Mull) - a well located close to the southern border of the study area. The simulator-calculated BHFP was higher than the recorded WHFP in wells such as the Blk25, Blk25U, Blk28, EberF, and EberU suggesting presence of excess gas and/or flow capacity. However in remaining wells, the BHFP was less than the WHFP, often hovering at 14.7 psi, suggesting that these wells are running out of gas in the post-1970 period under the current completion framework, i.e., fractures constrained to L4 in the post-1970.

Figure 40 displays the pressure distribution as of May 2006 along an east-west cross section across the HobEU well. The maximum pressure in L2 is 80 psi while at the well grid is at 30 psi. The maximum pressure in L4 is 200 psi (away from the well) while the well grid is at 57 psi. Figure 41 plots the gas in place over time in the top 6 layers of the reservoir model in the simulator. It shows that, as expected, the gas in place decreases over time in L1, L2, and L4. However, the gas in place in L3 and L5 increased over time indicating the movement of gas from adjacent layers into shale layers and the flow of gas and water out of shale layers into adjacent layers leaving residual gas in L3 and L5. This plot also shows that gas in place in L6 declines over time despite completions restrained to L4 in the post-1970 period. Thus, gas from L6 is able to travel through L5 and into the wells completed in L4 at vertical permeabilities set in the model for in Run 7.

4.8 RUN 8

Given the shortfall in simulator-calculated production in the wells Daniels (Dan), Hampston, and Towner (Town), post-1970 fractures in these wells were extended to L6 (Towanda) using ff = 1.0. Using ff = 1.0 across fractured intervals means that the

fracturing resulted in establishing communication with L5 and L6 layers but did not lead to productivity gains beyond a normal completion (such as perforation) in these layers. Also, many of the wells (stated in the section above) showed signs of excess gas in their drainage and thus a permeability multiplier of 0.8 was used on the initial permeability distribution (as in Run 1) in L6 (Towanda) and L8 (Ft. Riley). The permeability multiplier selected for L6 and L8 is based on the estimates made by comparing upscaled whole-core data and that predicted using facies-specific permeability correlations (Figure 15). Figures 42 and 43 shows the production/pressure matches at individual wells. The simulator-calculated production matched historic volumes at Hampston and Towner. Also, the match between the simulator-calculated FBHPs and the historic WHFPs improved at these 2 wells. However, simulator-calculated production at Daniels still is short of historic volumes though higher than that calculated in Run 7. Also, simulator-calculated cumulative production fell short of historic volumes in Schmelzel (Schml), Wilson (Wils), Muller (Mull), and Williams (Wilm).

4.9 RUN 9

It is evident from Figure 4.1d that the permeability distribution around Blackmer 28 (Blk28) in L4 (Winfield) is significantly higher than prevalent values elsewhere. These high permeability values cause the simulator-calculated gas production to match historic production volumes from this well in Run 1 and other subsequent runs while the simulator-calculated BHFPs remain greater than the WHFPs. Thus the permeability distribution in the drainage area around Blk28 was multiplied by 0.06 to reduce it to the same level as permeability at other wells in Winfield. Figure 44 shows that this localized permeability adjustment resulted in a production history match and a reduction in the calculated BHFPs bringing it closer, though still higher, to the historic WHFPs.

Well matches still show excess gas in many of the wells (Figures 42 and 43). Figure 45A shows that the upscaled vertical permeability (Kz) values (at HobEU) in the simulator model for L5 and L7 s are an order higher or greater than those of L1, L3, and L9. The initial estimates for Kxy in the fine-layer model were upscaled using Petrel's®

tensor upscaling routine and then facies-specific correlations related to the horizontal permeability (Kxy) were used to estimate the Kz in each of the layers input to the simulator. It is evident from various simulation runs that relatively high Kz allows migration of gas from zones below the completed (fractured) layers into the well. Figure 45B shows that significant volumes (about 8 bcf) of gas were produced out of L8 (Ft. Riley).

4.10 RUN 10

To reduce the availability of gas around most wells in the study area, the vertical permeability in L7 (B/Towanda) was reduced by multiplying the original permeability distribution by 0.1. Also, to increase production at Daniels (Dan) and Schmelzel (Schml) wells, ff factor (post 1970) was increased to 4.0 at Dan while the hydraulic fracturing in Schml was extended to L6 (post 1970) using ff = 1.0. Figures 46 and 47 show the resultant cumulative production and flowing pressure matches at individual wells. The production and pressure matches are close to historic values at most wells. However, wells such as EberF. EberU, Blackmer 25U, Blackmer 28, and Hoobler EU still show excess flow capacity as their BHFPs are higher than historic WHFPs. Muller (Mull) and Williams (Willm) are adjacent wells located at the southern border of the study area and both appear to run out of producible gas. The simulator-calculated production rates at the Mull well matches the post-1970 history though falling short during the pre-1970 production period.

4.11 RUN 11

In order to address excess production capacity in the above mentioned wells, adjustments were made in the effectiveness of hydraulic fracturing on production at select wells. At Blackmer 28 (Blk28), the matrix permeability in the drainage area was reduced by multiplying the permeability distribution (in Run 9) by 0.67 in order to bring the permeability values closer to its neighboring wells. Also, the ff was reduced to 3.0 (from 6.0) in the post-1970 period for hydraulic fracturing at this well constrained already to L4

(Winfield). For the wells Blackmer 25 (Blk25) and Blackmer 25U (Blk25U), the ff was reduced to 1.0 in the post-1970 period. Also, ff values in the post 1970 period were reduced to 2.0 at Ebersole, to 1.0 at Ebersole F and Ebersole U, and to 3.0 at Hoobler EU. The results of individual well production and pressure matches are shown in Figures 48 and 49. Figure 50 summarizes the quality of matches obtained against production and pressure histories at each well and also the presence or absence of production spikes when well flowed free of rate constraints. Close production and pressure history matches have been obtained at majority of the wells. However, most wells still show a production spike when released of flow constraints. Simulator-calculated production fell short of historic rates at two wells, namely Muller (Mull) and Williams (Willm), which are located at the southern border of the study area.

Figure 51 shows the average pore-volume weighted pressures at L1, L2, L4, L6, and L8 over the production life of the field. The table enclosed in this figure compares the simulator-calculated average pore-volume weighted reservoir pressure as of May 2006 with corresponding estimates of layer pressures from RFT tests carried out in and around the study area. Figure 52 shows that despite no wells being completed in L8 (Ft. Riley), about 6.4 bcf of gas has moved out of Ft. Riley to layers above and to wells completed in L6 (Towanda) and L4 (Winfield). The volume of gas flowing across shale layers is dictated by the vertical permeability assigned to the shale layers.

5.0 Conclusions

The intent of the simulation study was to evaluate robustness of a geomodel developed using an automated facies recognition technique anchored to a limited number of node wells in the study area, in this case only three in a 12-section area, and available facies-specific petrophysical data. The above mentioned geomodel served as the basis for this reservoir simulation study. The goal for this study was to see how closely the simulator could match the production and pressure histories of wells located in the geomodel with minimum modifications to the geomodel. Most geomodel modifications were applied all over the study area, such as using layer specific permeability multipliers. The only well

specific modifications made included varying productivity and reach of the hydraulic fractures.

1. Out of 16 wells, good matches with production histories were obtained at 13 wells.
2. Close to good matches were obtained with flowing pressure histories at 12 out of the 16 wells in the study area.
3. Small to high production spikes were visible at seven out of 12 producing wells. Production spikes were not visible at the three wells where the simulator-calculated production fell short of historic volumes.
4. The pore-volume weighted average layer pressures in L1 (Herrington), L2 (Krider), L4 (Winfield), L6 (Towanda), and L8 (Ft. Riley) matched closely with corresponding estimated pressures from available RFT data.
5. It appears that the reservoir is more complex than the model input to the simulator because some of the wells show presence of excess flow capacity while others remain short of gas. The complexity of the reservoir is further revealed by a closer look at individual well performances such as Blackmer 28 (Blk28), where the simulator-calculated bottom-hole flowing pressures exceed historic surface flowing pressures indicating excess flow capacity and yet the same well fails to meet the historically recorded gas volumes after the year 2000. Also, the simulator is unable to match production history at Muller (Mull) even in the pre-1970 period. Thus, any field-wide increase in layer permeability or layer OGIP to obtain production match will result in excess flow capacity at wells where production history matches have already been achieved.
6. None of the wells have been completed in Ft. Riley (L8) and yet 6.4 bcf of gas flowed out of this layer to layers above and to the wells completed in Winfield (L4) and Towanda (L6). Based on the layer-specific gas-in-place plots, it appears that fluid movement is taking place across the shale layers with vertical permeability playing a critical role in determining the amount of fluid flow in shale.

References

Dubois, M.K., A.P. Byrnes, T.R. Carr, G.C. Bohling, and J.H. Doveton, 2006, Multiscale geologic and petrophysical modeling of the giant Hugoton gas field (Permian), Kansas and Oklahoma, in P. M. Harris and L. J. Weber, eds., Giant reservoirs of the world: From rocks to reservoir characterization and modeling: AAPG Memoir 88 (in press).

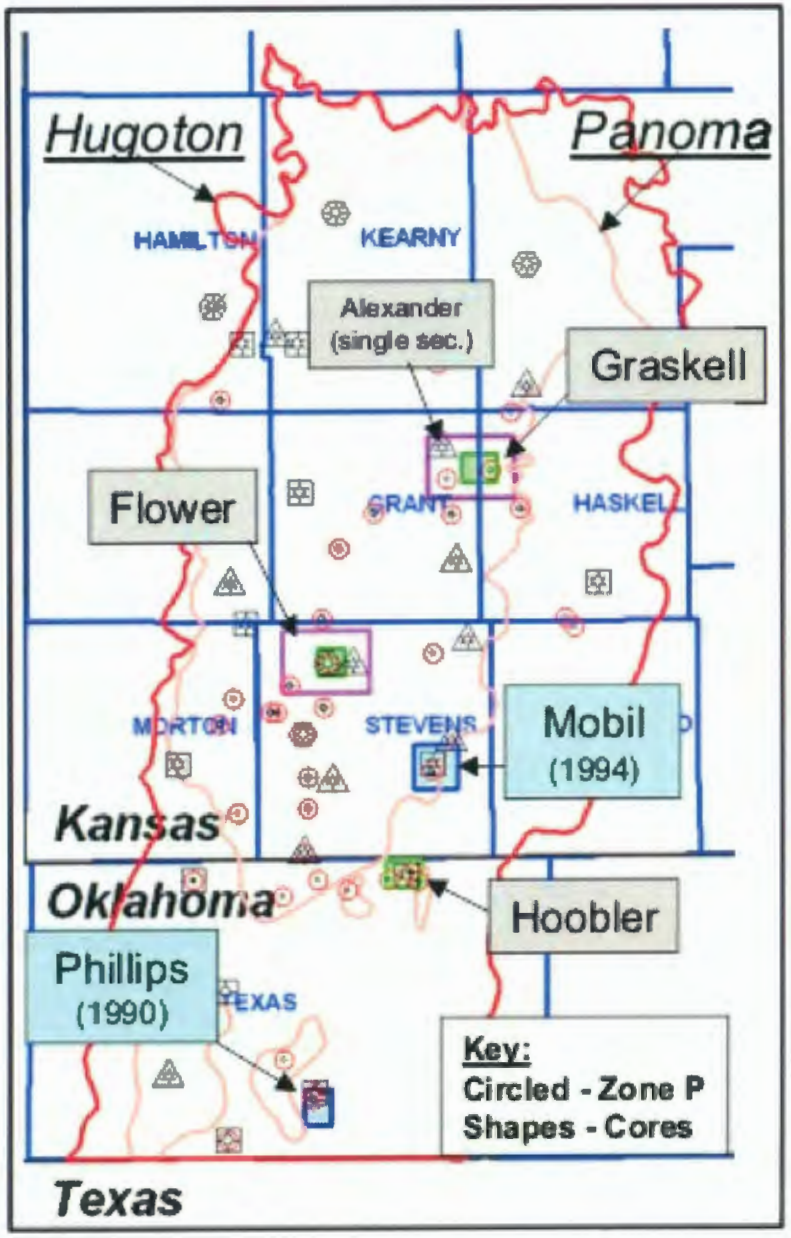

Hugoton
Panoma
HAMILTON
KEARNY
Alexander
(single sec.)
Graskell
Flower
GRANT
HASKELL
MORTON
STEVENS
Mobil
(1994)
Kansas
Oklahoma
Hoobler
Phillips
(1990)
TEXAS
Key:
Circled - Zone P
Shapes - Cores
Texas

Figure 1

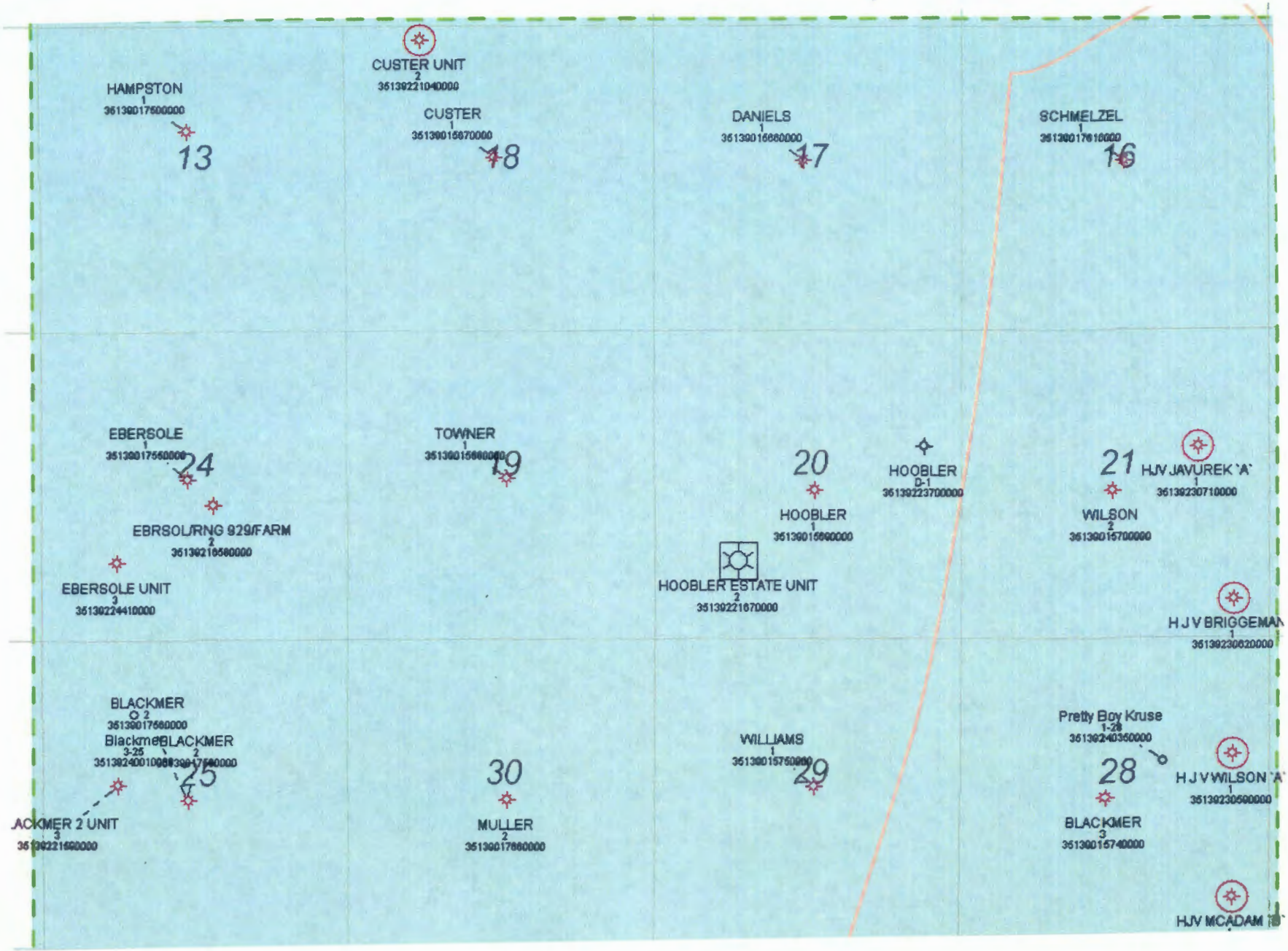

HAMPSTON
1
35139017500000
13
CUSTER UNIT
2
35139221040000
CUSTER
1
35139015670000
18
DANIELS
1
35139015660000
17
SCHMELZEL
1
35139017610000
16
EBERSOLE
1
35139017560000
24
EBRSOL/RNG 929/FARM
2
35139216560000
EBERSOLE UNIT
3
35139224410000
TOWNER
1
35139015680000
19
20
HOOBLER
1
35139015690000
HOOBLER
D-1
35139223700000
HOOBLER ESTATE UNIT
2
35139221670000
21
WILSON
2
35139015700000
HJV JAVUREK `A`
1
35139230710000
HJV BRIGGEMAN
1
35139230620000
BLACKMER
2
35139017560000
Blackmer
3-25
BLACKMER
2
25
ACKMER 2 UNIT
3
30
MULLER
2
35139017660000
WILLIAMS
1
35139015750000
29
Pretty Boy Kruse
1-28
35139240360000
28
BLACKMER
3
35139015740000
HJV WILSON `A`
1
35139230590000
HJV MCADAM

Figure 2

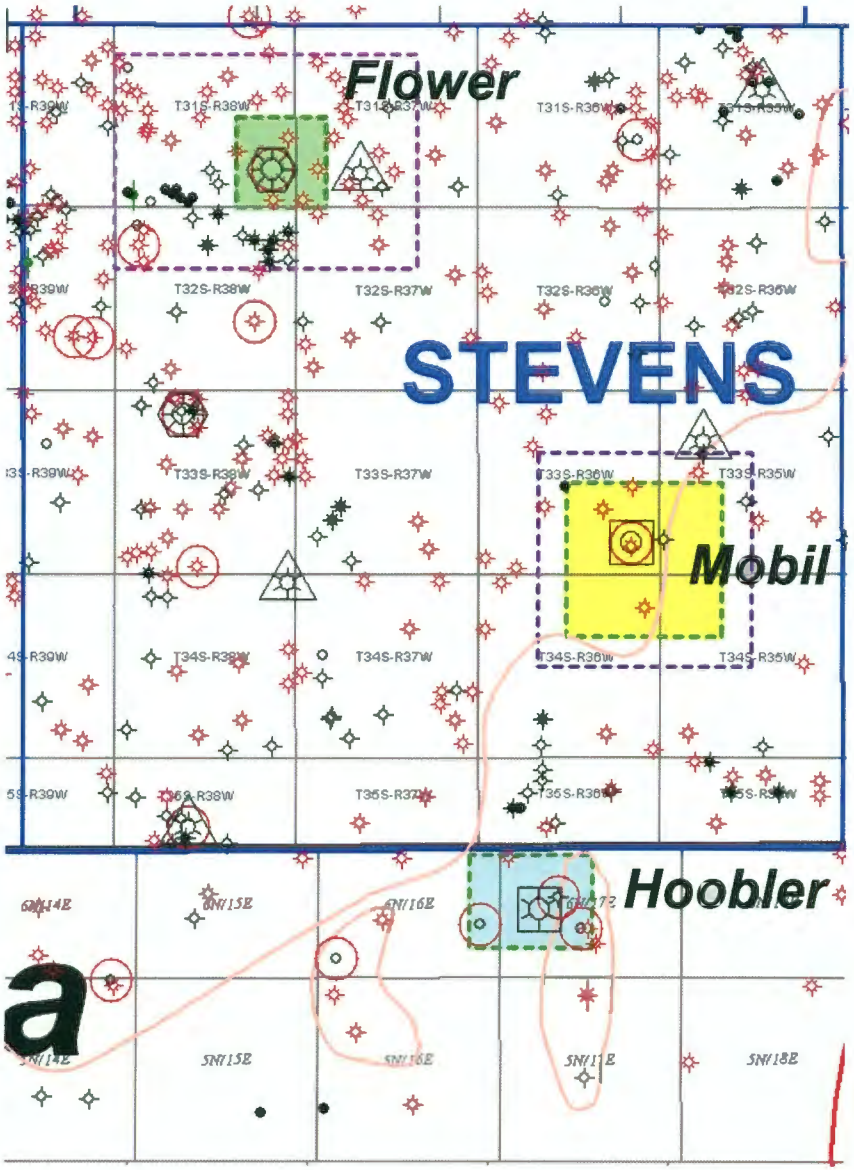
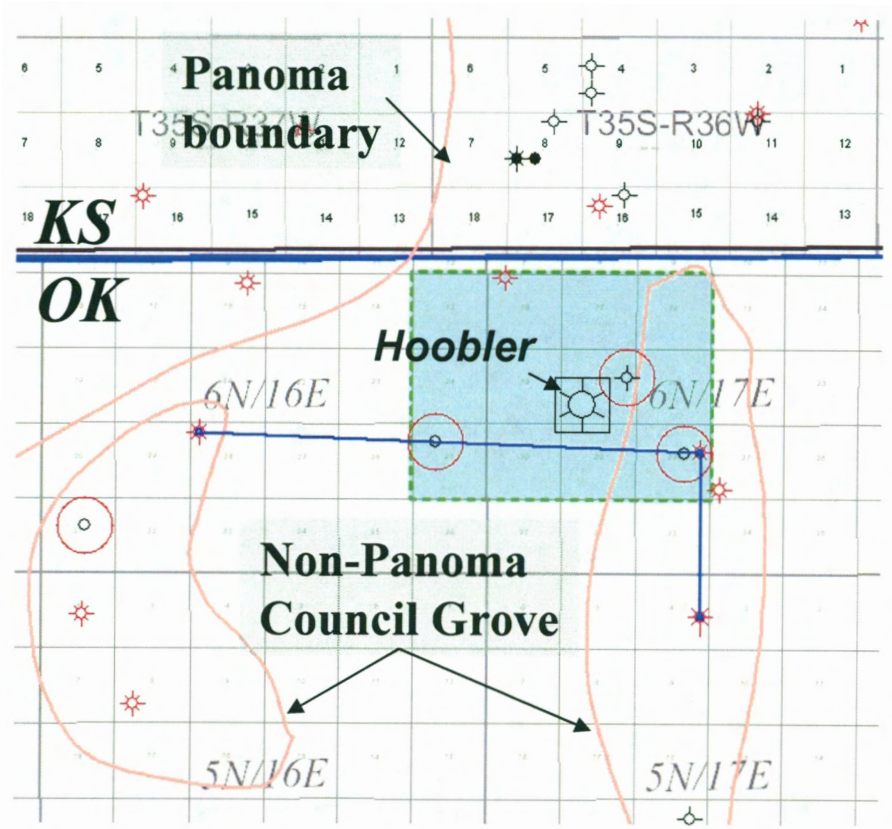


Figure 3 – Node wells for Geomod 4 (full field model) in Hoobler area. Wells with with pressure data are circled.

Current "node" wells



○ Zone pressure available

Figure 4

Hoobler model extraction

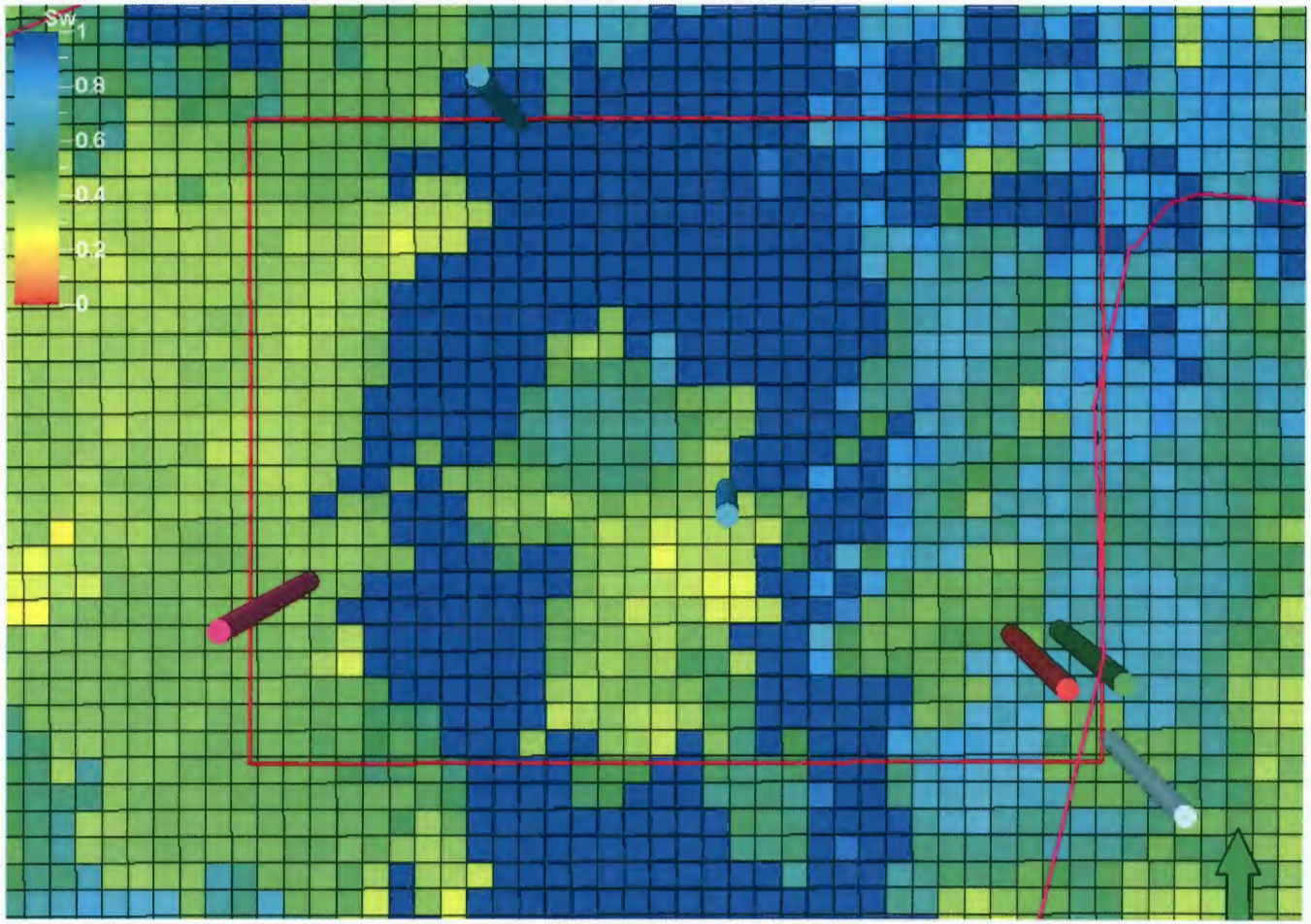


Figure 5 - Map view of water saturation for top layer in the Herington in Geomod4. Outline of Hoobler area is in red. Wells shown are the model "node" wells.

Upscaling Petrophysical Properties

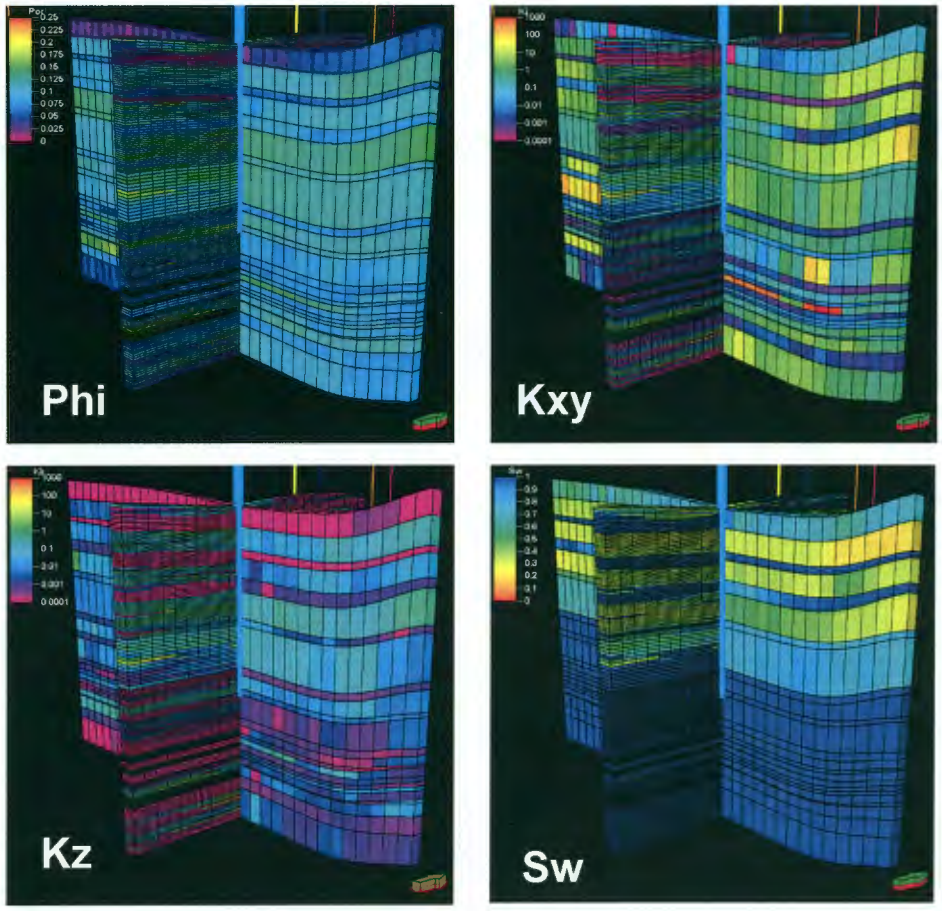


Figure 6 - Porosity, permeability, and water saturation upscaled from 269 layers to 24 layers, one layer per zone in the Chase and Council Grove.

Hoobler 11-layer model -OGIP

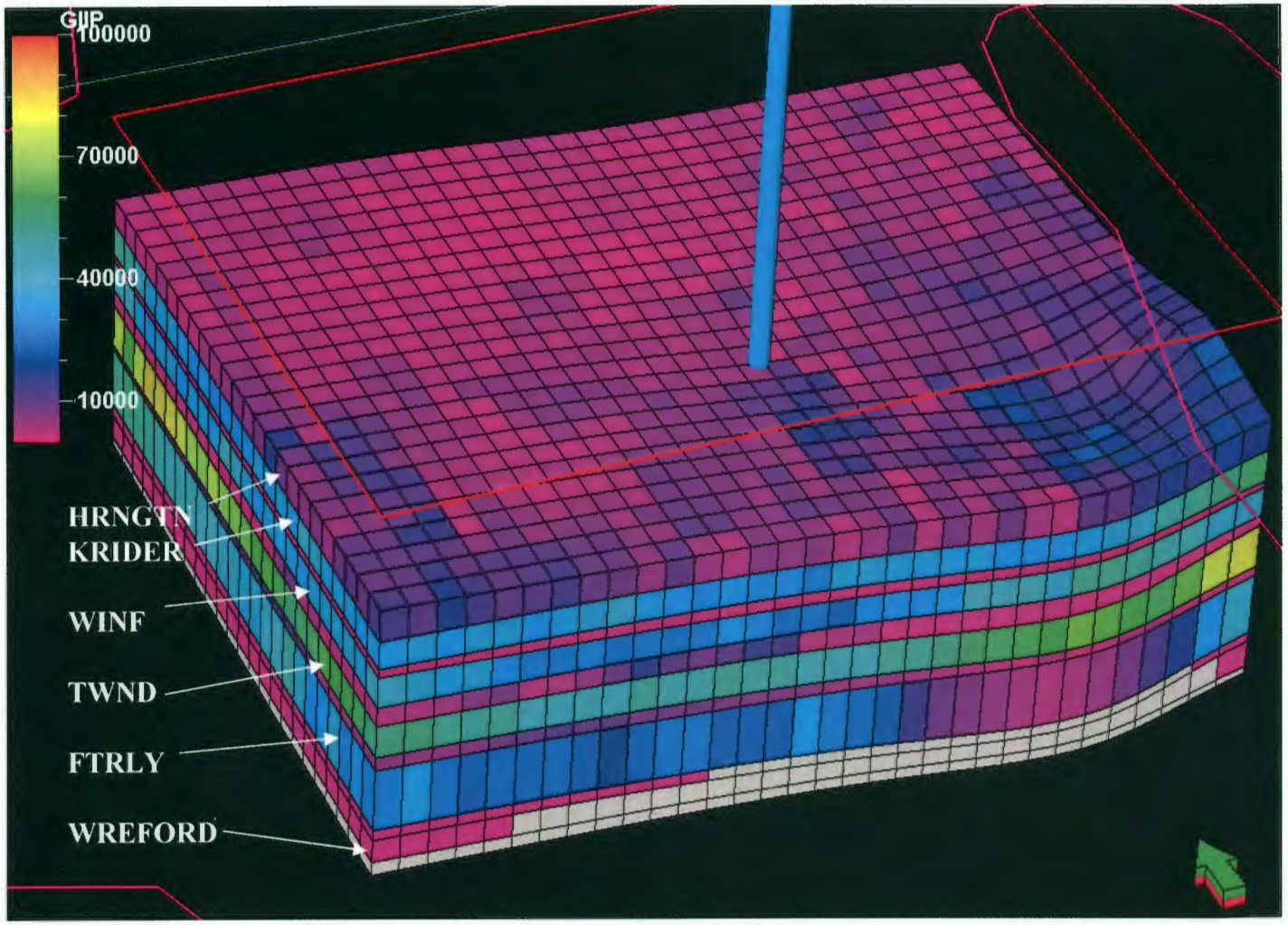


Figure 7 - Distribution of GIP for the 11-layer model with a FWL at +65 feet above sea level. Hoobler wellbore is shown.

Hoobler 11-layer model – other properties

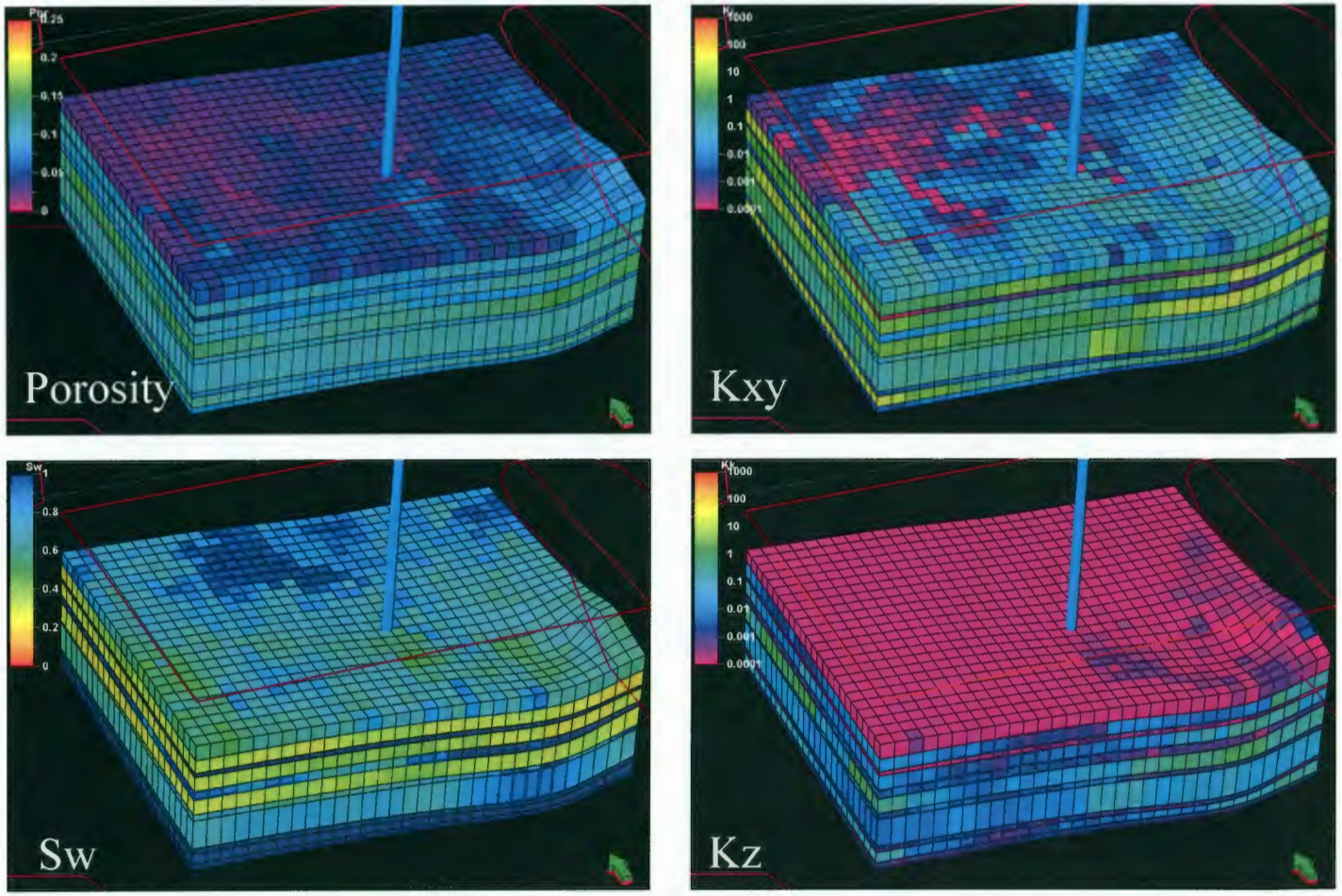


Figure 8 - Properties in the Hoobler 11-layer model. Hoobler wellbore is shown.

$$PHI_CORR = A + B*DPHI + C*NPHI$$

	Intercept A	PHID B	PHIN C
Facies 1 & 2	0.018	0.843	0.000
Facies 3 & 4	0.019	0.662	0.000
Facies 5 & 7 & 8	4.278	0.400	0.209
Facies 6	0.000	0.500	0.500
Facies 9	8.918	0.447	0.131
Facies 10	4.484	0.524	0.135

Figure 9 - Regression analysis of core-to-log porosity results in an equation and set of constants by lithofacies.

Assumed PVT properties:			
Reference pressure	465	psi	
Rock compressibility	0.000002	1/psi	(assumed)
Reservoir temp	90	F	
Gas gravity (Air = 1.0)	0.715		
Water salinity	110,000	ppm	

Figure 10

Layer	Depth	WC Phi	WC K, md
Krider	2753	7.7	0.18
Krider	2754	7.9	0.15
Krider	2755	8.3	0.11
Krider	2756	10.8	0.2
Krider	2757	11.8	2.08
Krider	2758	12.5	3.14
Krider	2759	14.4	3.67
Krider	2760	14.7	4.23
Krider	2761	14.4	4.23
Krider	2762	14.6	4.23
Krider	2763	14.4	4.23
Krider	2764	13.3	1.56
Krider	2765	11.1	0.36
Krider	2766	12.1	1.46
Krider	2767	12.7	4.5
Krider	2768	12.1	1.45
Krider	2769	11.8	0.9
Krider	2770	13.1	1.85
Krider	2771	13.6	1.76
Krider	2772	10.1	0.59
Krider	2773	10.8	0.83
Krider	2774	11.4	1.29
Krider	2775	10.7	0.82
Krider	2776	12.4	1.65
Krider	2777	11.5	1.76
Krider	2778	11.3	1.98
Krider	2779	12.1	5.78
Krider	2780	13	3.73
Krider	2781	12.2	3.29
Krider	2782	12.6	3.43
Krider	2783	10.2	1.8
Krider	2784	10.9	1.46
Krider	2785	9.8	1.21
Krider	2786	12.8	2.92
Krider	2788	11	5.1
Krider	2789	9.9	4.5
Krider	2790	10.1	3.09
Krider	2791	9.6	1.71
Krider	2792	8	0.35

L2 (Krider) Mean K = 2.24 md

Added multiplier of 2 can be used

Layer	Depth	WC Phi	WC K, md
Winfield	2811	4.5	0.02
Winfield	2812	6.7	0.22
Winfield	2813	3.1	0.06
Winfield	2814	3.3	0.88
Winfield	2815	4.2	0.35
Winfield	2816	4.3	37.86
Winfield	2817	6	0.81
Winfield	2818	7.7	0.36
Winfield	2822	12.9	0.73
Winfield	2823	13.2	1.84
Winfield	2824	9.1	0.73
Winfield	2825	6.9	0.1
Winfield	2826	7.4	0.03
Winfield	2827	7.5	0.12
Winfield	2828	10	1.37
Winfield	2829	8.7	0.44
Winfield	2830	7	0.14
Winfield	2831	5.7	0.06
Winfield	2832	11.4	0.92
Winfield	2833	16.8	8.35
Winfield	2834	13.9	13.94
Winfield	2835	17.3	13.95
Winfield	2836	14.3	4.12
Winfield	2837	12.5	2.89
Winfield	2838	12.1	3.5
Winfield	2839	10.7	2.26
Winfield	2840	8.4	0.94
Winfield	2841	5.5	0.09
Winfield	2842	6.9	0.02

Avg with 37.86	3.34
Avg without 37.86	2.11

Added multiplier of 2 can be used

(Except drainage of Blk28)

Mean K = 0.93 md

Layer	Depth	WC Phi	WC K, md
Towanda	2868	15.2	0.37
Towanda	2869	15.7	0.57
Towanda	2870	16.3	0.57
Towanda	2871	17	0.57
Towanda	2872	17.4	0.65
Towanda	2873	17.4	1
Towanda	2874	17.5	1.75
Towanda	2875	17.5	1.75
Towanda	2876	17.1	1.07
Towanda	2877	15	0.53
Towanda	2878	12.8	0.42
Towanda	2879	13.1	0.21
Towanda	2880	13	0.2
Towanda	2881	13	0.16
Towanda	2882	11.2	0.07
Towanda	2883	10.8	0.04
Towanda	2884	11.5	0.04
Towanda	2885	12.3	0.08
Towanda	2886	12.3	0.14
Towanda	2887	12.6	0.28
Towanda	2888	13.5	0.53
Towanda	2889	14.3	1.21
Towanda	2890	14.1	1.76
Towanda	2891	14.5	1.76
Towanda	2892	15.4	1.99
Towanda	2893	16	3.97
Towanda	2894	15.5	0.83
Towanda	2895	12.7	0.53
Towanda	2896	13.2	0.53
Towanda	2897	14.5	0.56
Towanda	2898	14.4	1.1
Towanda	2899	14.2	1.87
Towanda	2900	14.1	1.99
Towanda	2901	14	1.99
Towanda	2902	13.9	1.99
Towanda	2903	13.8	1.87
Towanda	2904	13.7	1.27
Towanda	2905	13.6	0.89
Towanda	2906	13.1	0.39
Towanda	2907	12.6	0.39
Towanda	2908	13.7	0.6
Towanda	2909	13.5	0.82
Towanda	2910	13.5	0.44
Towanda	2912	15.4	0.39
Towanda	2913	16.5	0.78
Towanda	2914	15.7	1.87
Towanda	2915	14	0.83

Figure 11

Crossplot of *in situ* Klinkenberg permeability versus *in situ* porosity for whole core identified as fractured (asterisks), whole core that were not identified as fractured but may contain microfractures (grey circle), and unfractured core plugs (black triangle). Permeabilities shown were either measured or routine values were corrected to *in situ* conditions using the equation presented in Figure 3.2c.

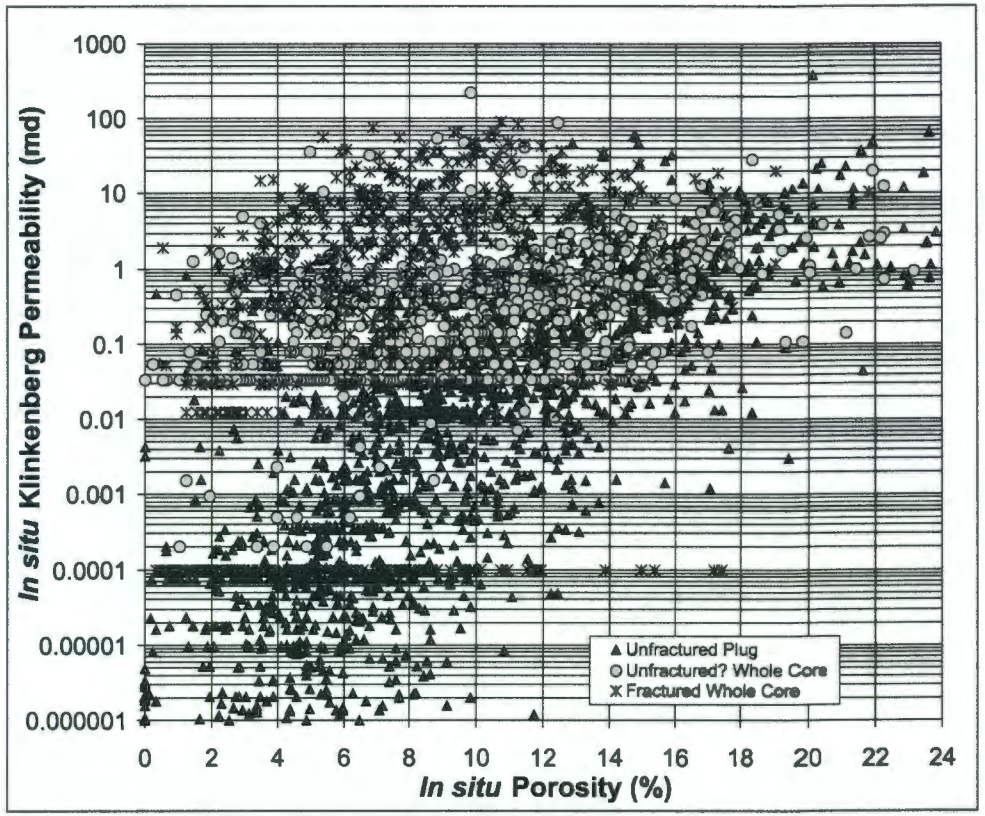
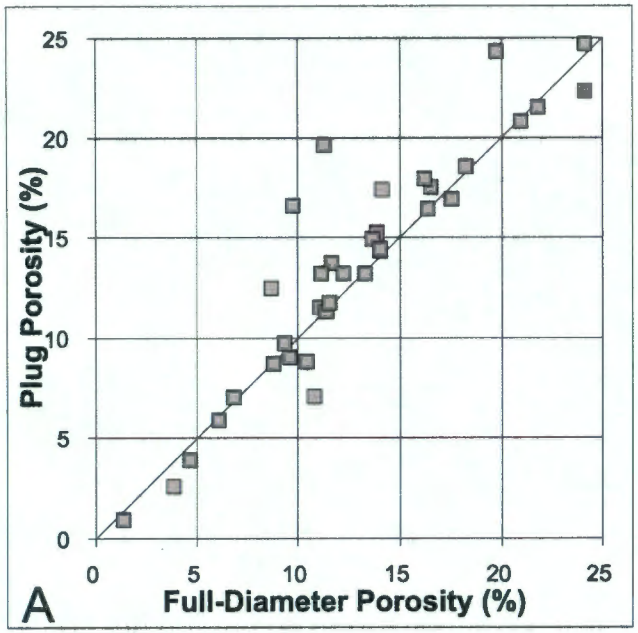


Figure 12


25
20
15
10
5
0
Plug Porosity (%)
0
5
10
15
20
25
A
Full-Diameter Porosity (%)

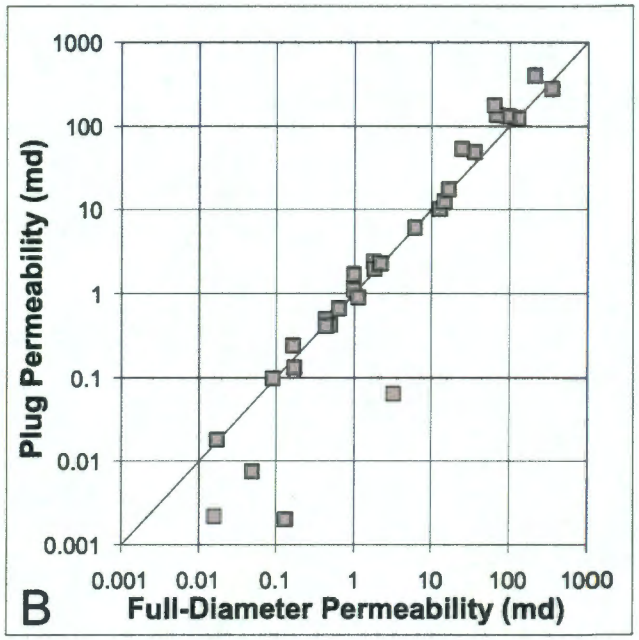

1000
100
10
1
0.1
0.01
0.001
Plug Permeability (md)
0.001
0.01
0.1
1
10
100
1000
B
Full-Diameter Permeability (md)

Figure 13

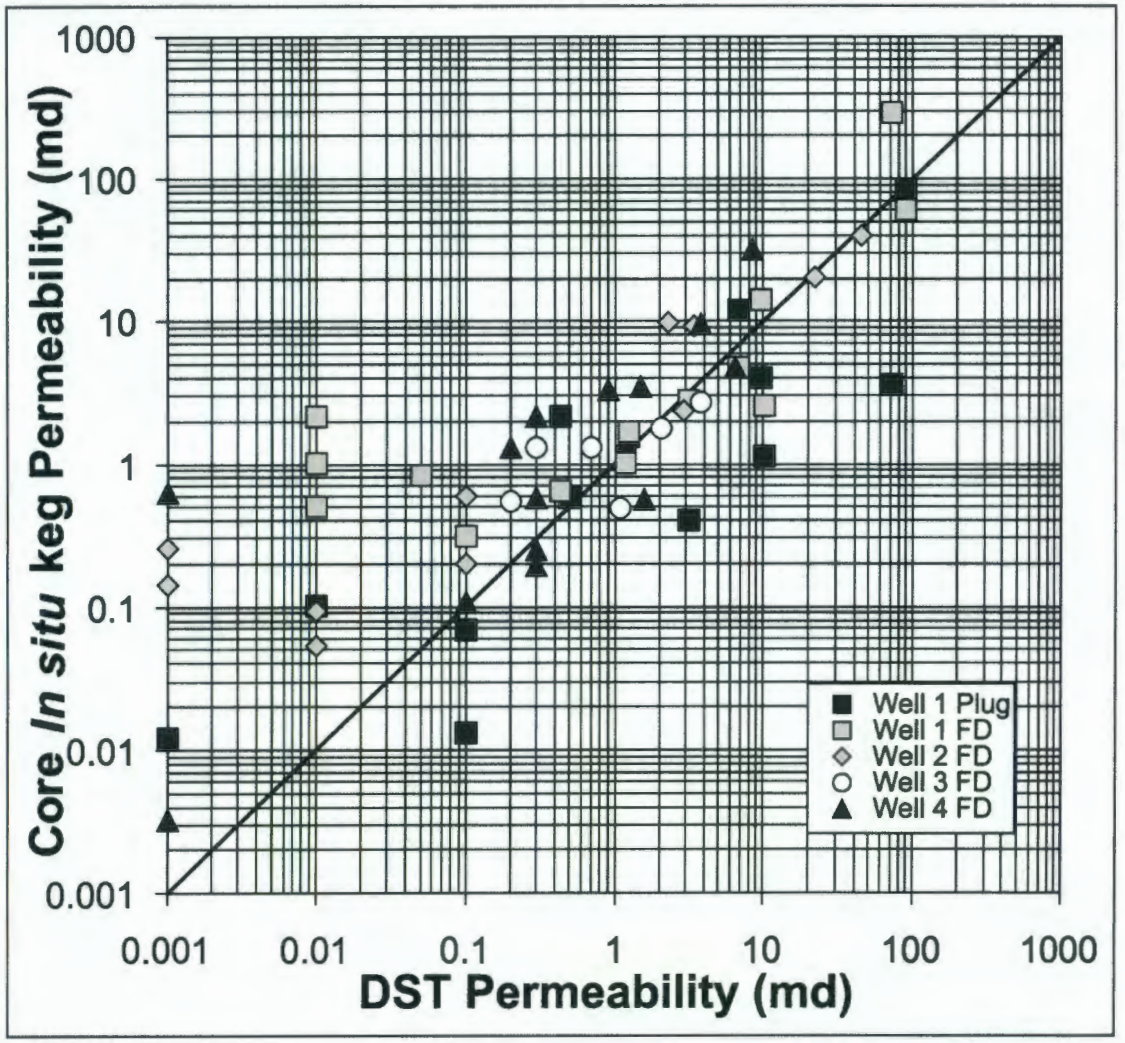

1000
100
10
1
0.1
0.01
0.001
Core *In situ* keg Permeability (md)
0.001
0.01
0.1
1
10
100
1000
DST Permeability (md)
Well 1 Plug
Well 1 FD
Well 2 FD
Well 3 FD
Well 4 FD

Figure 14

Model	Formation	Core Kxy (mean)	Model Kxy	Model Kz	Multiplier
1	Herrington	0.286	0.0274	0.000005	10.4
2	Krider	2.246	1.7833	0.036	1.3
3	Odell	0.067	0.0005	0.000007	134.0
4	Winfield	3.348	2.2702	0.00138	1.5
5	Gage	0.359	0.0077	0.0016	46.6
6	Towanda	0.928	1.126	0.0586	0.8
7	B/TWND	0.3	0.0385	0.00323	7.8
8	Ft. Riley	0.215	0.2929	0.0273	0.7
9	Matfield	1.518	0.0032	0.00068	474.4
10	Wreford	0.315	1.21	0.027	0.3
11	A1-SH		0.0029	0.0011	

A multiplier significantly greater than 1.0, i.e., 10.4, is calculated for this layer where specifies-specific K-phi trends predict permeability to be less than 0.5 md.

Exception: A multiplier close to 1.0, i.e., 0.7, is calculated for this layer where the core Kxy is less than 0.5 md (i.e., 0.215).

Figure 15

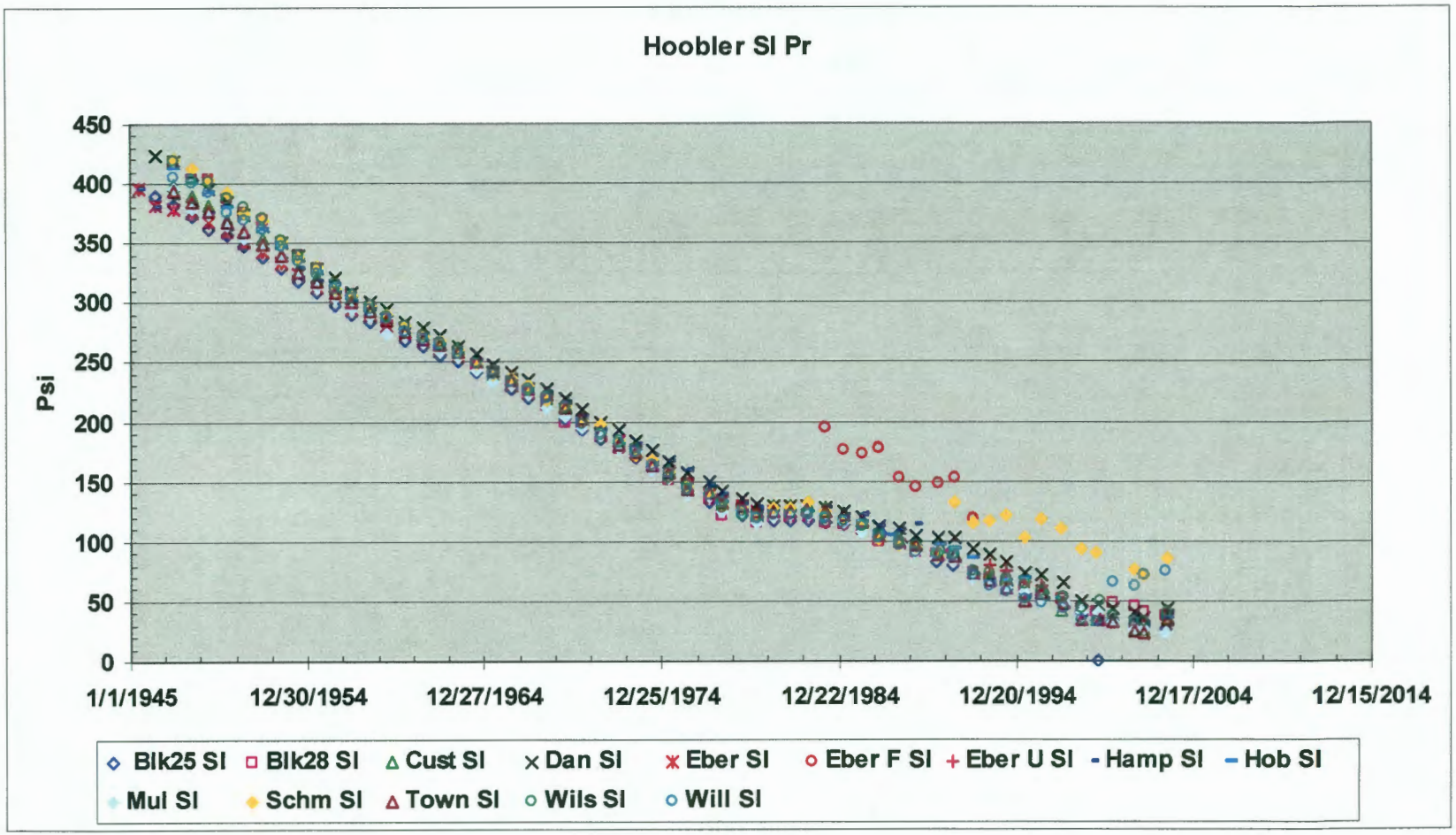

Hoobler Sl Pr
Psi
450
400
350
300
250
200
150
100
50
0
1/1/1945
12/30/1954
12/27/1964
12/25/1974
12/22/1984
12/20/1994
12/17/2004
12/15/2014
Blk25 Sl
Blk28 Sl
Cust Sl
Dan Sl
Eber Sl
Eber F Sl
Eber U Sl
Hamp Sl
Hob Sl
Mul Sl
Schm Sl
Town Sl
Wils Sl
Will Sl

Figure 16

Sp gr of gas	0.715	(Air = 1)	Ppc (dependent on gas gr)	662	psia		enter data
Assume WHSP	420	psi	Tpc (dependent on gas gr)	380	R		Calculation
Well depth	2750	ft					
			Tbg head static temp	60	F	520	R
Est BHSP - Ist Pws	448.9	psi	Bottom hole static temp	95	F	555	R
	Ist Iteration		Avg wellbore pr	434.4	psi		
			Avg wellbore temp	537.5	R		
			Ppr	0.66			
			Tpr	1.41			
			Z	0.92			
			s	0.149109			
			2nd Pws =	452.5	psi		
	2nd Iteration						
			Avg wellbore pr	436.3	psi		
			Ppr	0.66			
			Tpr	1.41			
			Z	0.92	**(within the limits of readability of the chart)**		
			s	0.149109 (unchanged from previous calculation)			
			Thus, Pws (BHSP) =	**452.5 psi**			

(Assume starting res pr as 450 psi)

Figure 17

Layer	Name	Petrel OGIP, bcf	Sim OGIP, bcf
1	Hrngtn	4	4.2
2	Krider	31	30.8
3	Odell	0	0.0123
4	Winf	23	23.1
5	Gage	2	1.89
6	Twnd	42	42.85
7	B/Twnd	3	3.04
8	Ftrly	23	25.19
9	Matfield	0	0
10	Wreford	0	0.0097
11	A1_SH	0	0
At 450 psi, bcf OGIP		128	131.1

Figure 18

						Total Prod, bcf	70.13
	Well	Sim Name	Start Prod	X address	Y address	Perf Layers	Cum, mcf
1	Blackmer 25	Blk25	9/1/1946	3	20	1-2-3-4	6,321,500
2	Blackmer 25U	Blk25U	4/1/1987	1	19	1-2-3-4	
3	Blackmer 28	Blk28	2/1/1947	27	20		3,731,024
4	Custer	Cust	2/1/1947	12	3		6,020,519
5	Daniels	Dan	7/1/1946	20	4		8,356,932
6	Ebersole	Eber	7/1/1941	4	11	2-3-4	5,278,760
7	Ebersole F	EberF	11/1/1982	4	12	1-2-3-4	271,689
8	Ebersole U	EberU	12/1/1992	2	13	2-3-4	903,085
9	Hampston	Hamp	5/1/1941	4	2	1-2-3-4	9,230,934
10	Hobbler	Hob	1/1/1947	20	12		4,436,418
11	HobbE	HobEU	6/1/1987	18	14	1-2-3-4	
12	Muller	Mull	10/1/1946	12	20	1-2-3-4	5,539,541
13	Schmelzel	Schml	12/1/1946	28	4	1-2-3-4	7,345,449
14	Towner	Town	9/1/1946	12	12		4,532,704
15	Willams	Willm	2/1/1947	20	20		4,021,503
16	Wilson	Wils	2/1/1947	28	12		4,137,886

Figure 19

							Total Prod, bcf	70.13
	Well	Sim Name	Start Prod	X address	Y address	Perf Layers	Spud date	Cum, mcf
1	Blk25	Blk25	9/1/1946	3	20	1-2-3-4	7/25/1946	6,321,500
2	Blk25U	Blk25U	4/1/1987	1	19	1-2-3-4	1/27/1987	
3	Blk28	Blk28	2/1/1947	27	20		1/1/1947	3,731,024
4	Custer	Cust	2/1/1947	12	3		1/1/1947	6,020,519
5	Daniels	Dan	7/1/1946	20	4		1/1/1946	8,356,932
6	Ebersole	Eber	7/1/1941	4	11	2-3-4	5/21/1940	5,278,760
7	Ebersole F	EberF	11/1/1982	4	12	1-2-3-4	5/29/1982	271,689
8	Ebersole U	EberU	12/1/1992	2	13	2-3-4	9/11/1992	903,085
9	Hampston	Hamp	5/1/1941	4	2	1-2-3-4	3/19/1940	9,230,934
10	Hobbler	Hob	1/1/1947	20	12		1/1/1947	4,436,418
11	HobbE	HobEU	6/1/1987	18	14	1-2-3-4	5/8/1987	
12	Muller	Mull	10/1/1946	12	20	1-2-3-4	8/22/1946	5,539,541
13	Schmelzel	Schml	12/1/1946	28	4	1-2-3-4	10/26/1946	7,345,449
14	Towner	Town	9/1/1946	12	12		1/1/1946	4,532,704
15	Willams	Willm	2/1/1947	20	20		1/1/1947	4,021,503
16	Wilson	Wils	2/1/1947	28	12		1/1/1946	4,137,886

	OGIP in top 4 layers, bcf	58.1		
Layer	Name	Marty's OGIP	Sim OGIP	Comments
1	Hrngtn	4	4.2	
2	Krider	31	30.8	
3	Odell	0	0.0123	Increasing OGIP with trime
4	Winf	23	23.1	

Figure 20



Run 6 – 11 layer model, ff = 6, K multi on pay

Figure 21

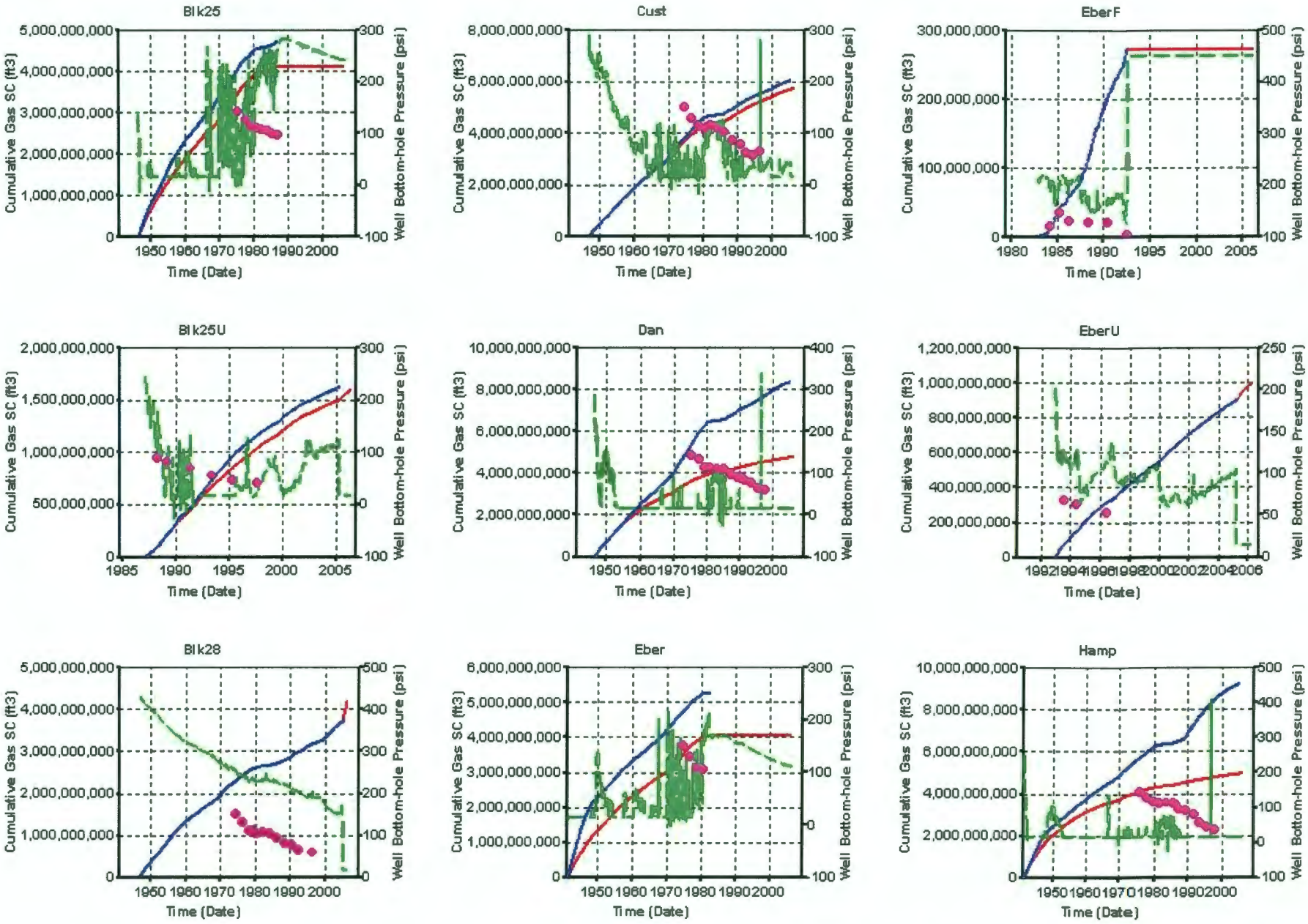
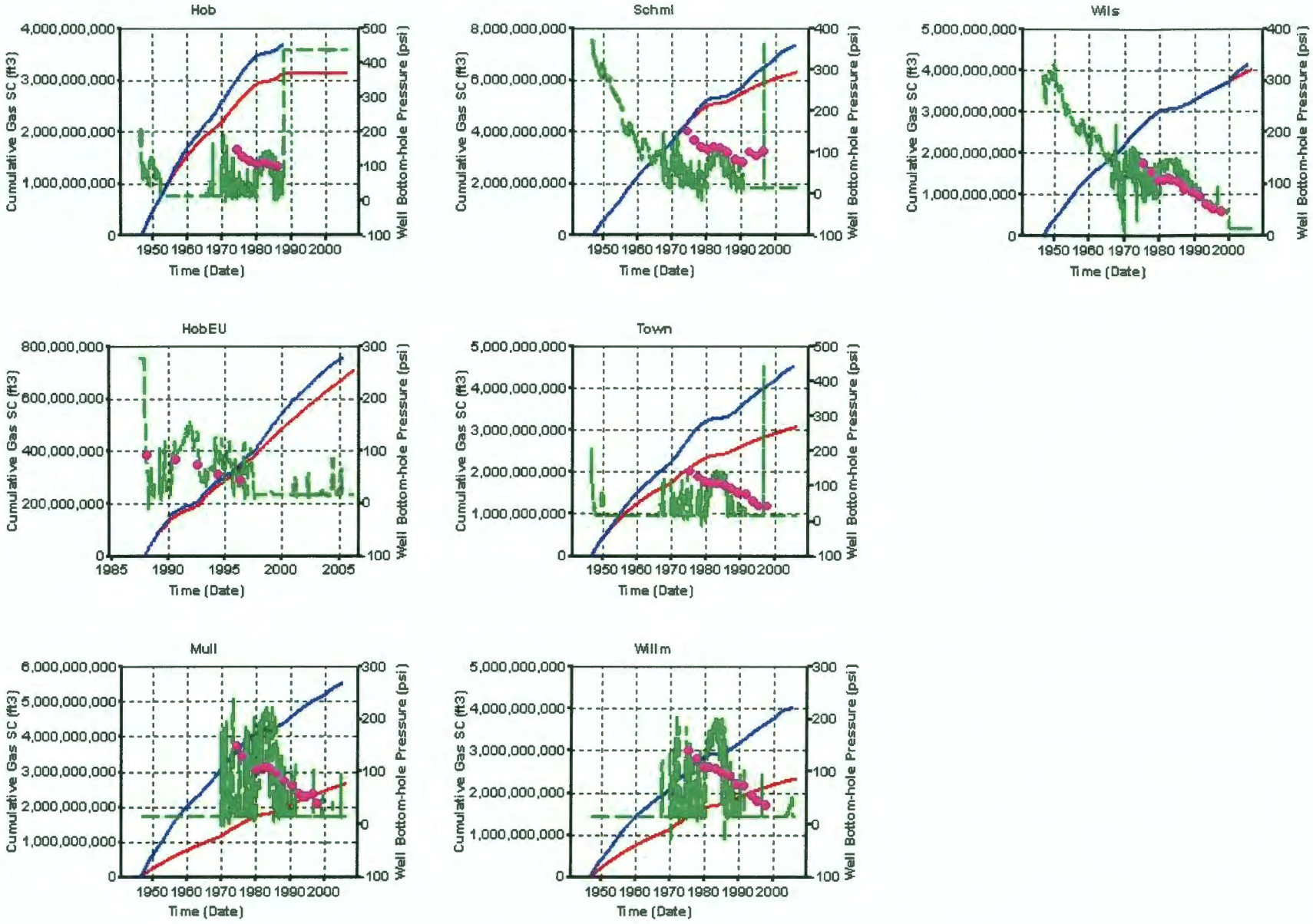


Figure 22

Sim 6 – 11 Layer model, ff = 6, K multi on pay

Blue – Prod his, Red – Sim Prod, Green – Sim FBHP, Magenta – Pr His



Sim 6 – L11, ff = 6, K multi on pay

Blue – Prod his, Red – Sim Prod, Green – Sim FBHP, Magenta – Pr His

Figure 23

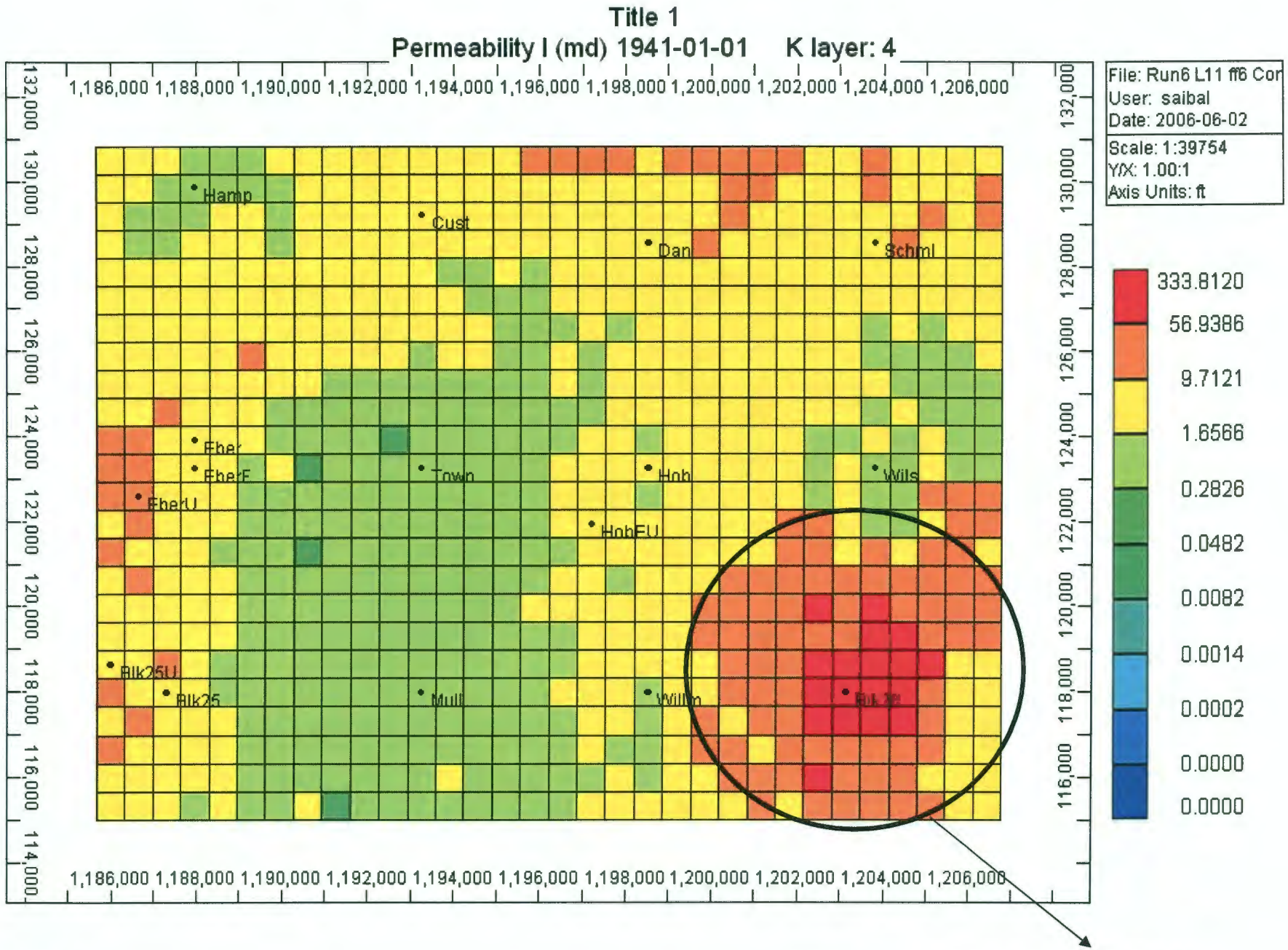


Figure 24

Permeability bull's eye in L4 near Blk28

RFT Pressures - Hoobler

If we assume the following:

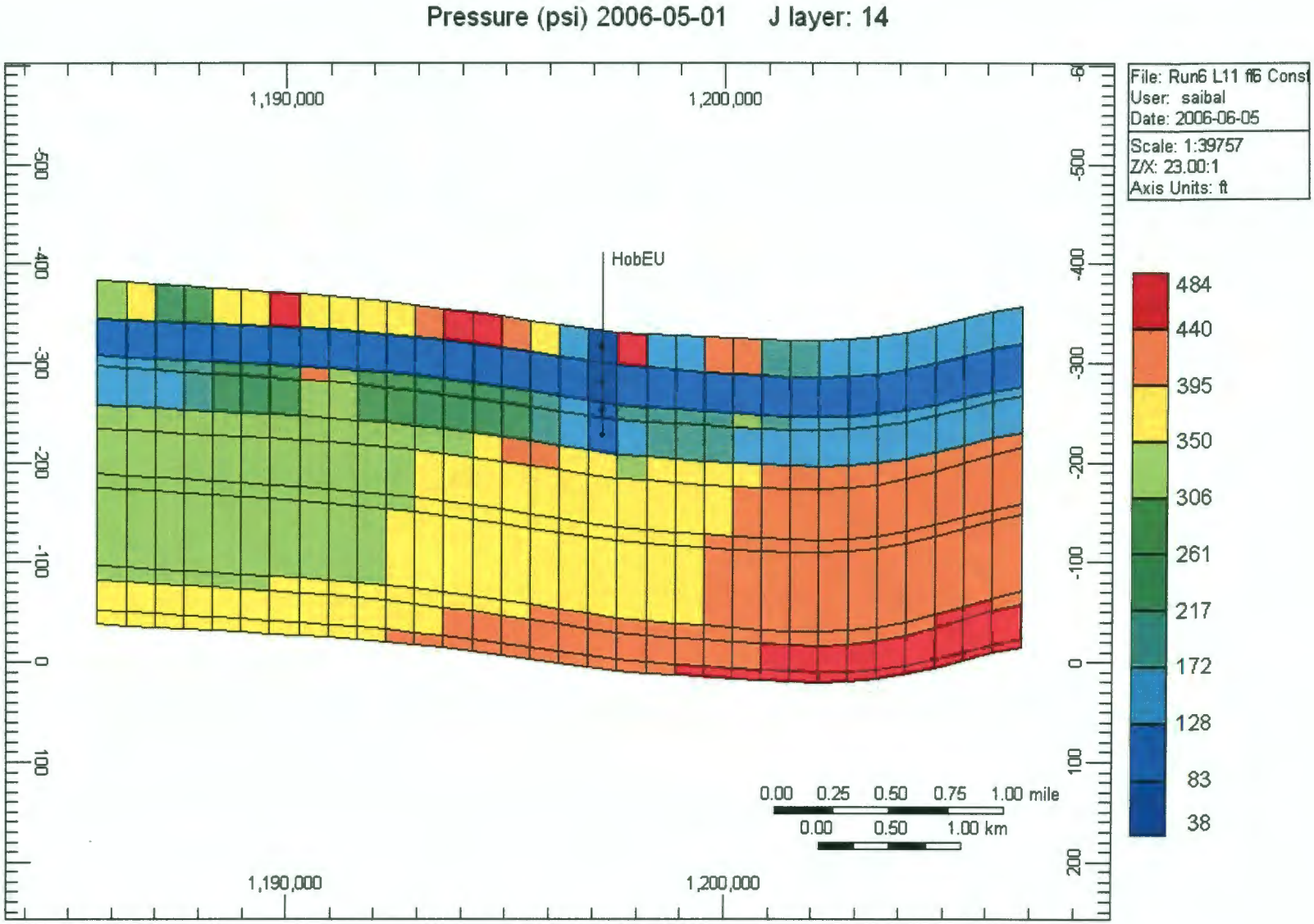
1. **WHSIP adjusted to BHP is the likely lowest pressure, highest permeability zone.**
2. **RFT's are likely to be too high by a considerable margin**
3. **Towanda was not regularly completed**
4. **Krider and Winfield have approximately equal permeability and depletion.**
5. **Initial BHP = 450 psig (adjusted from IWHSIP)**

The following pressures may be expected at individual layers as of 2005:

Herrington	**200+ psi**	**Probably poorly drained. No test info.**
Krider	**40-60 psi**	
Winfield	**40-60 psi**	
Towanda	**150-300 psi**	**Variable. Dependant on communication.**
Ft Riley	**450 psi**	**Not drained; too far below completed intervals**

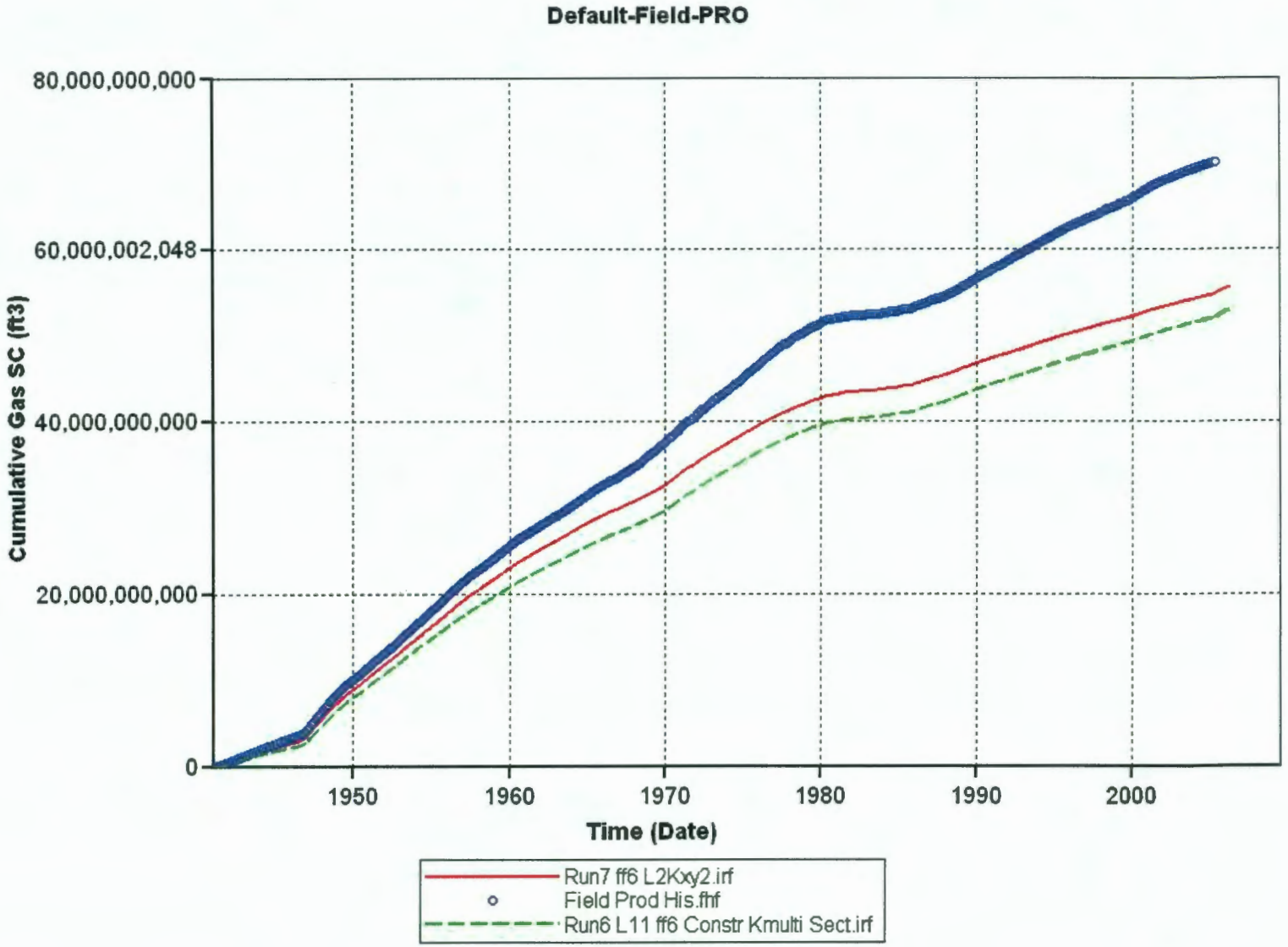
(above are best guesses and should be considered a starting point)

Figure 25



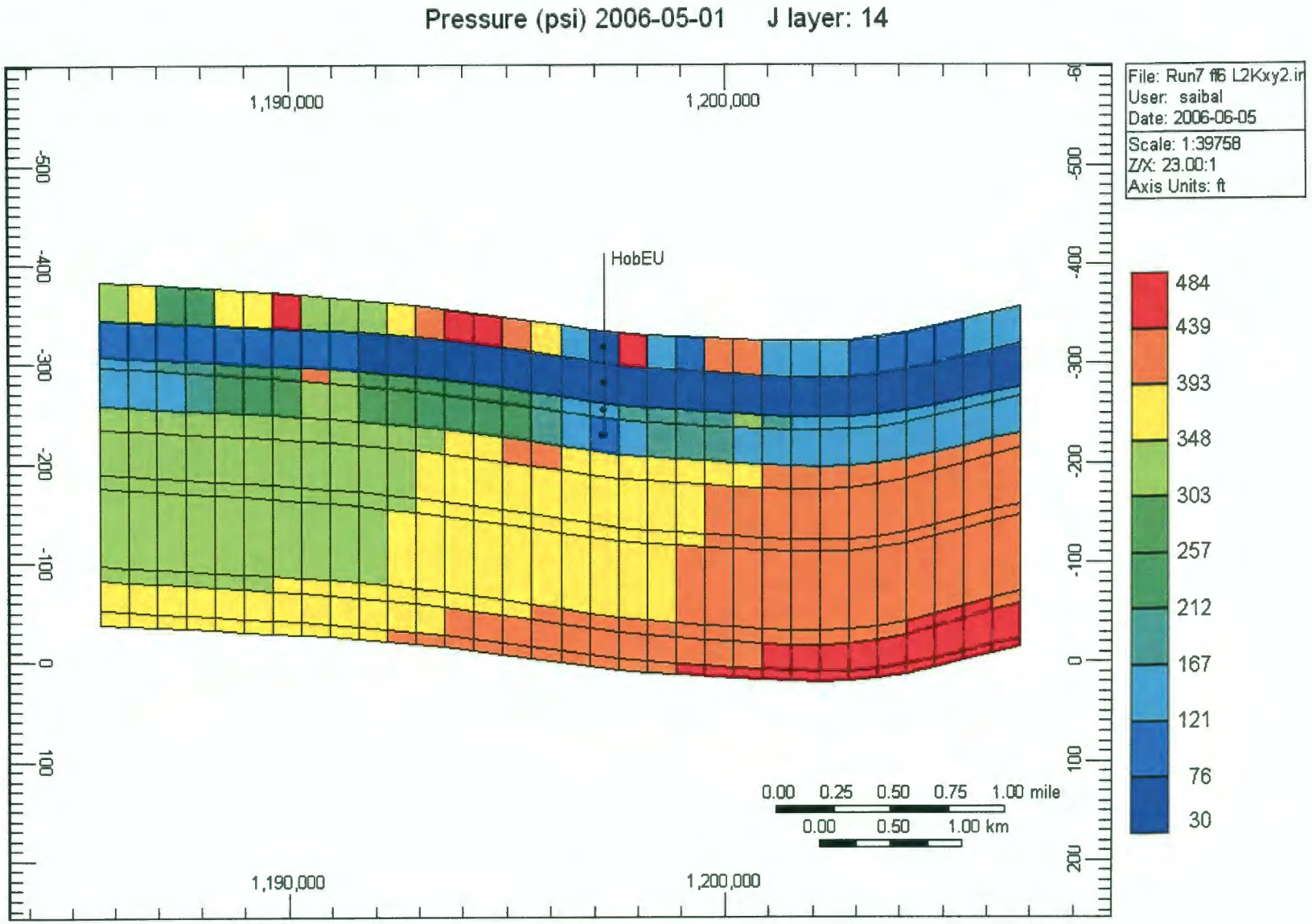
Sim 6 – L11, ff = 6, K multi on pay

Figure 26



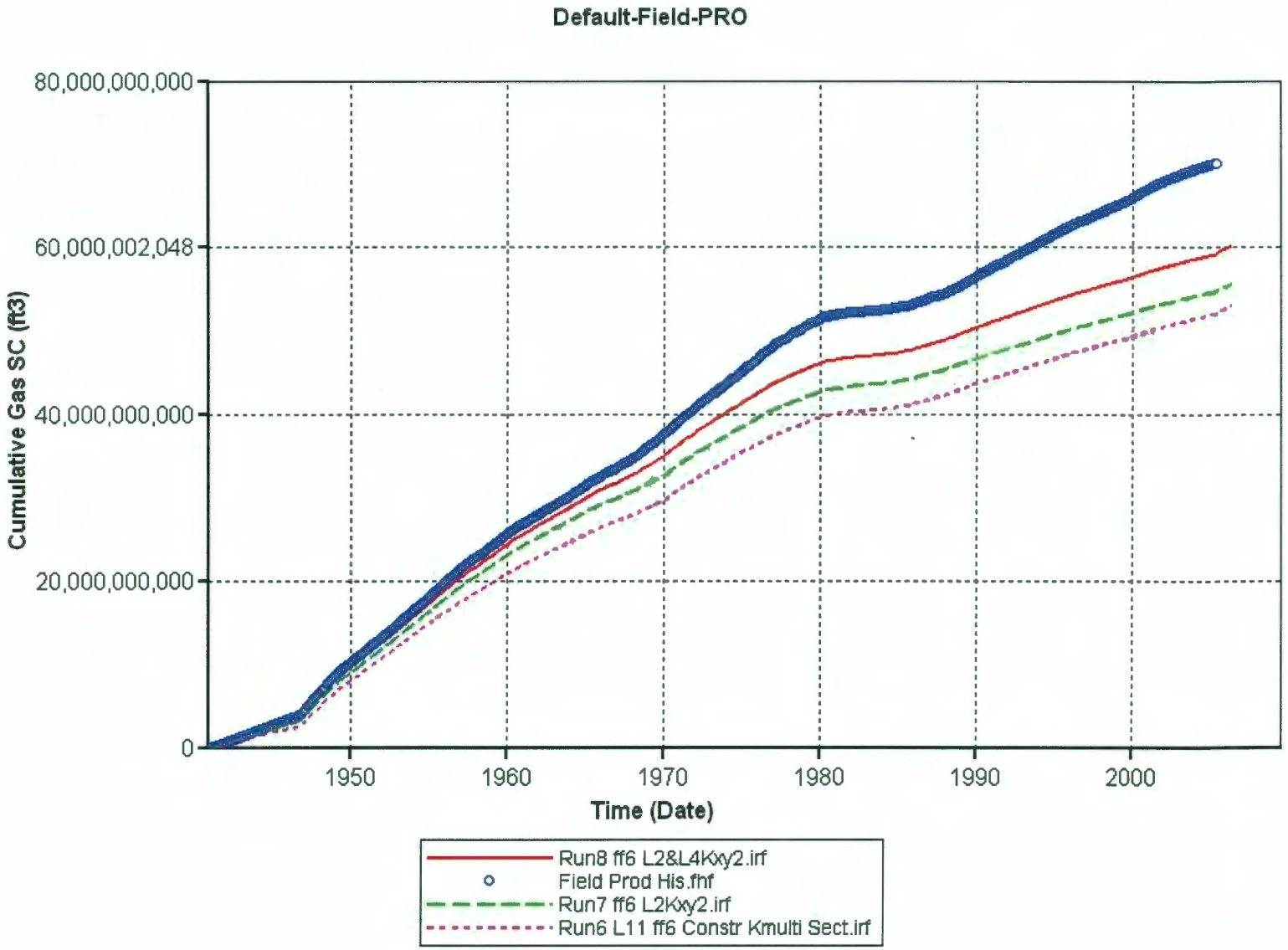
Sim 7: L2 (Krider) Kxy*2 (on starting multiplier)

Figure 27



Sim 7: L2 (Krider) Kxy*2 (additional)

Figure 28



Sim 8: L2 (Krider) and L4 (Winfield) Kxy*2 (on starting multiplier)

Figure 29

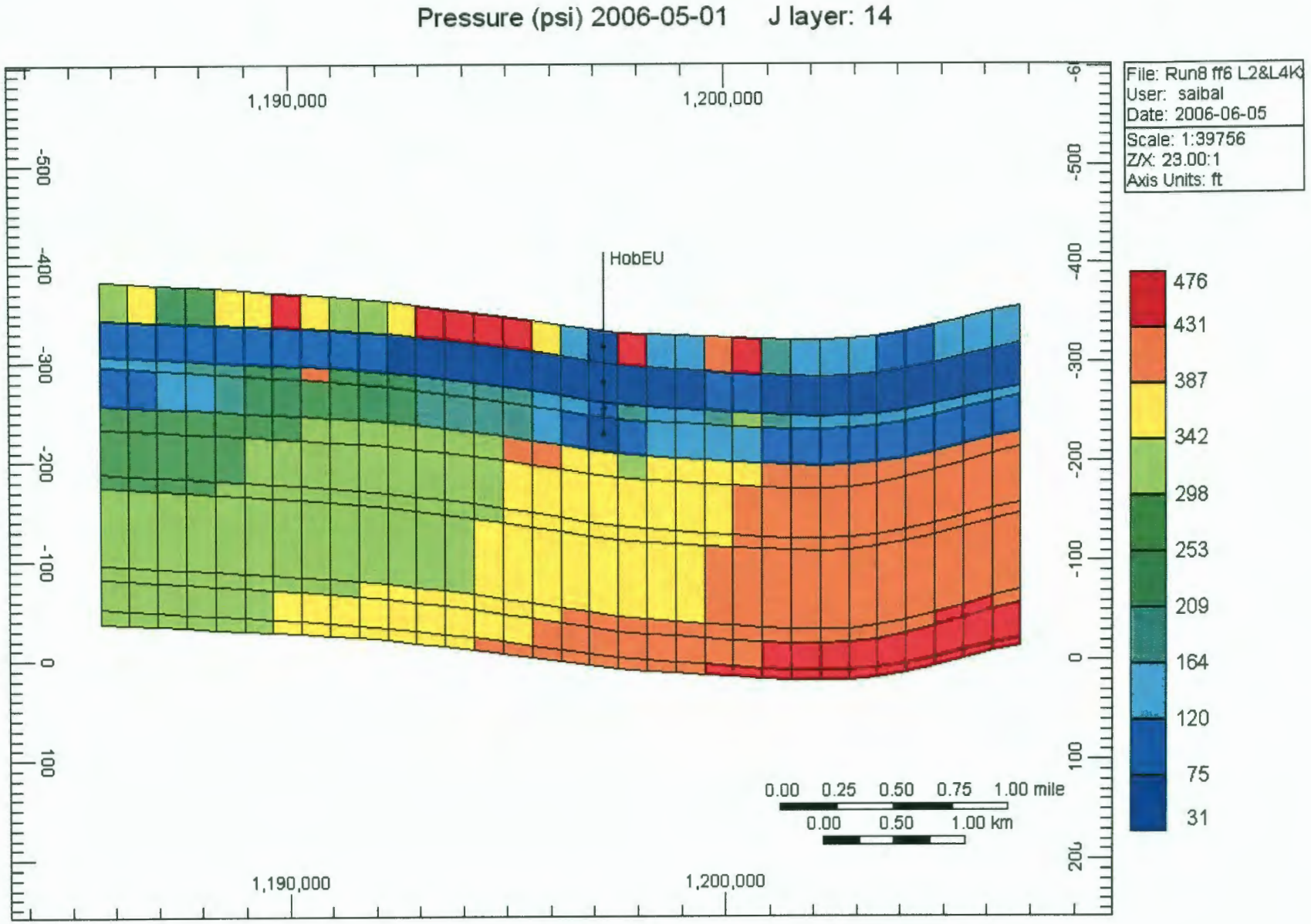
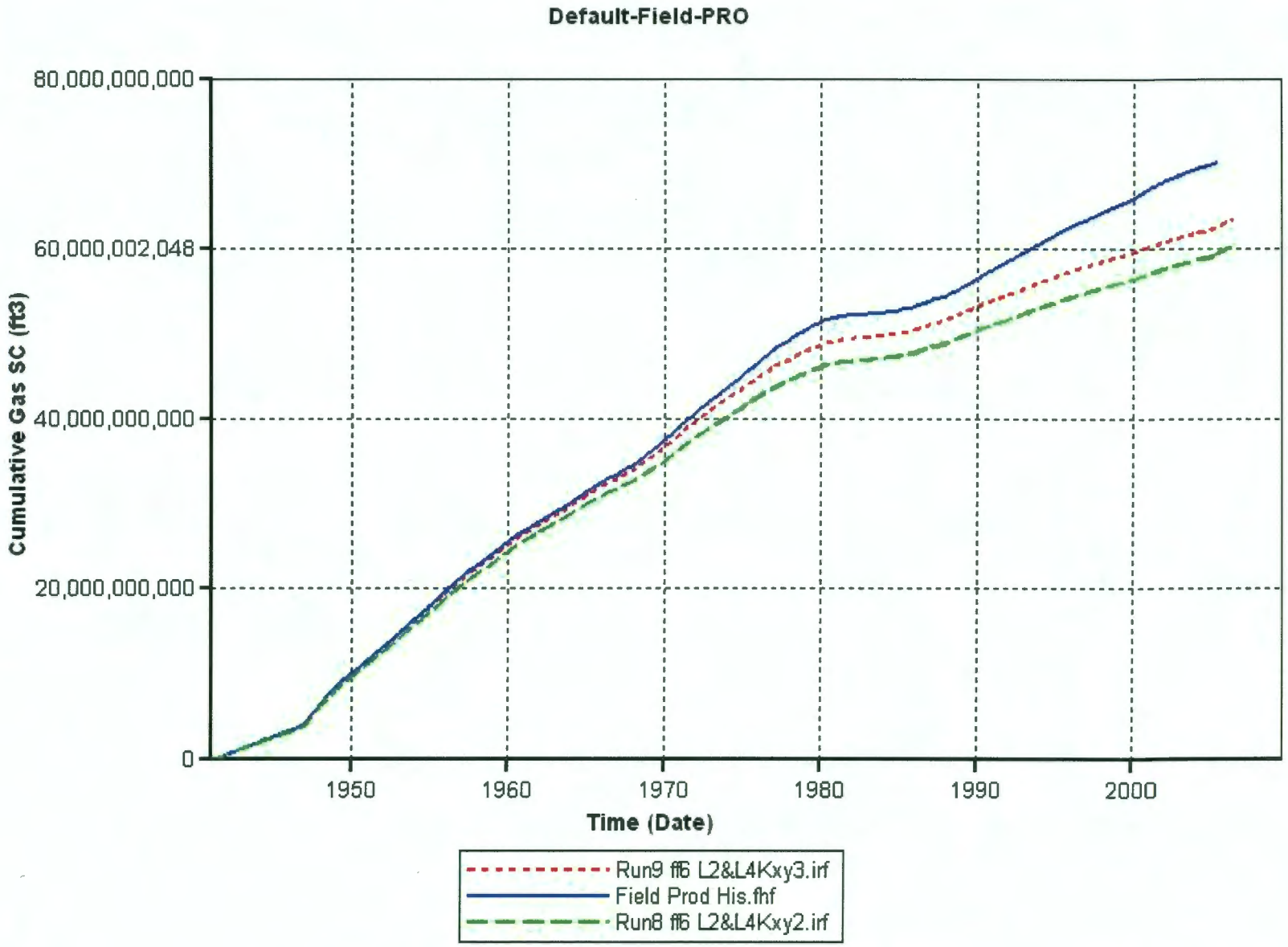


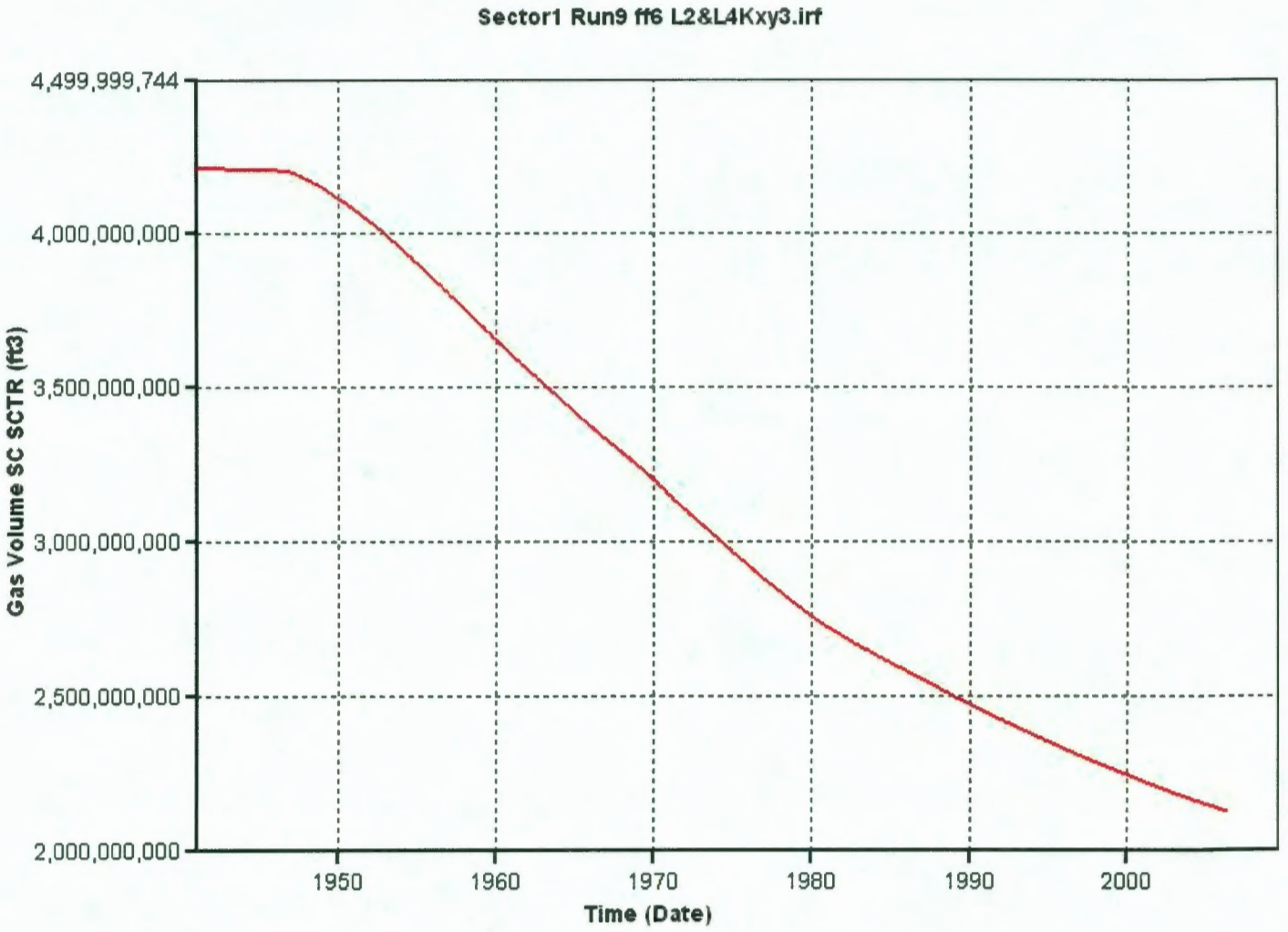
Figure 30

Sim 8: L2 (Krider) and L4(Winfield) Kxy*2 (on starting multiplier)



Sim 9: L2 (Krider) and L4 (Winfield) Kxy*3 (on starting multiplier)

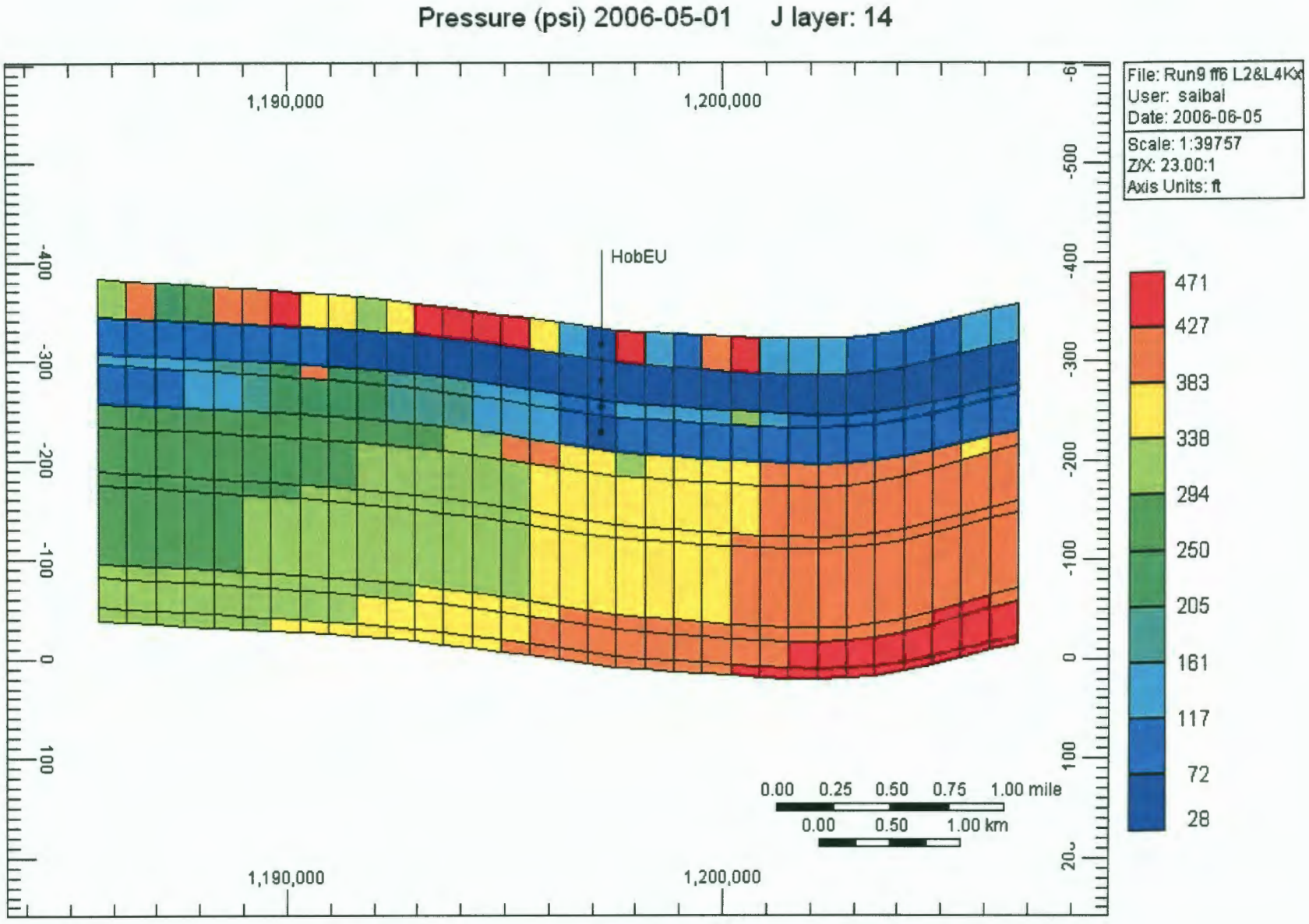
Figure 31



Run 9: L2 (Krider) and L4 (Winfield) Kxy*3 (on starting multiplier)

As of 1970, there is 3.25 bcf gas in place in L1 (Herrington).

Figure 32



Sim 9: L2 (Krider) and L4 (Winfield) Kxy*3 (on starting multiplier)

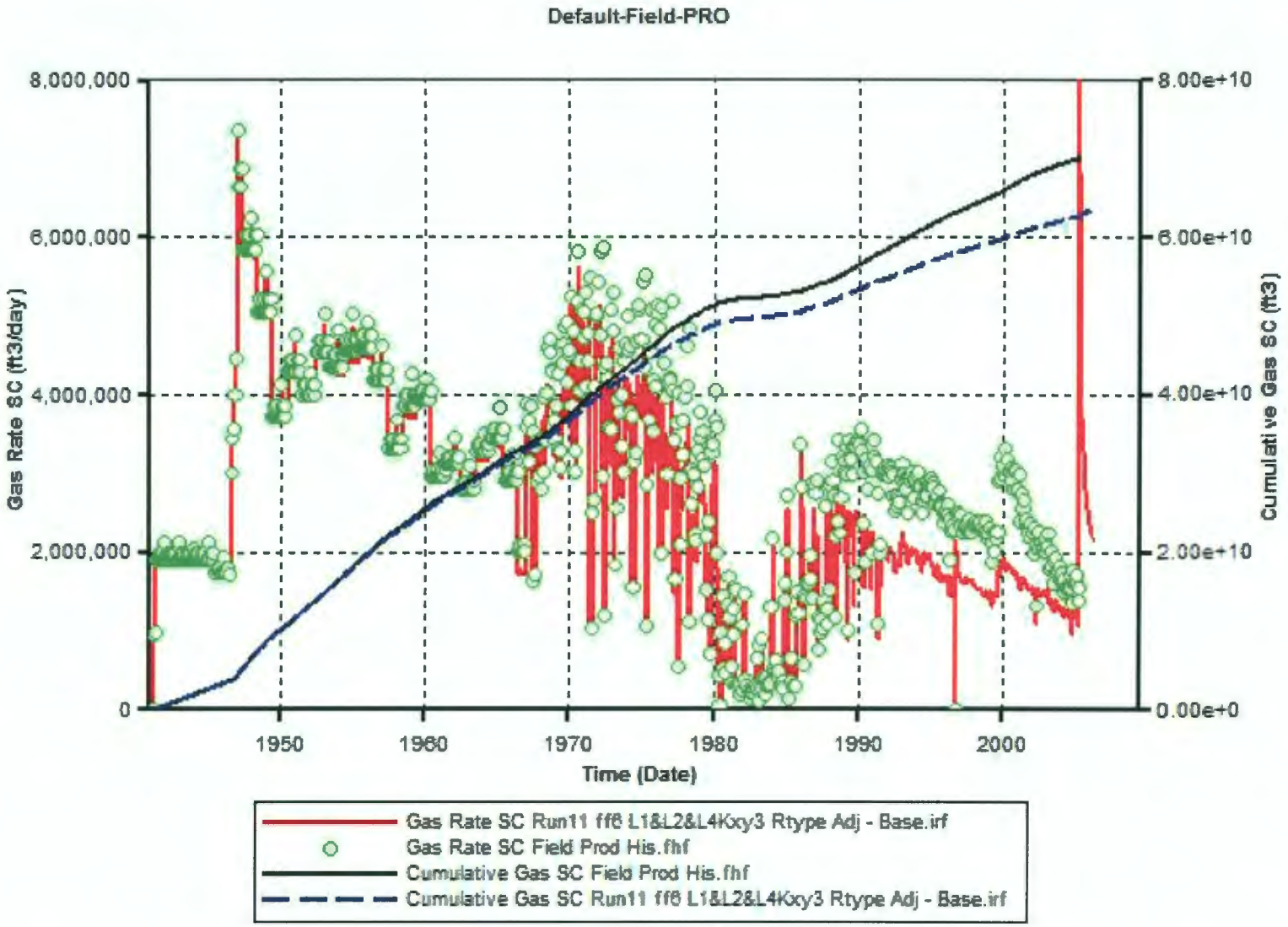
Figure 33

Layer	Depth	WC Phi	WC K, md
Herrington	2721	14.3	1.2
Herrington	2722	14.6	1.37
Herrington	2723	13.7	1.46
Herrington	2724	12.4	1.46
Herrington	2725	10.3	0.54
Herrington	2726	10.9	0.19
Herrington	2727	8.3	0.08
Herrington	2736	6.5	0.01
Herrington	2737	6.8	0.03
Herrington	2738	7.1	0.05
Herrington	2739	6.6	0.02
Herrington	2740	5.9	0.06
Herrington	2741	5.9	0.06
Herrington	2742	5.7	0.02
Herrington	2743	5.3	0.01
Herrington	2744	5.4	0.02
Herrington	2745	6.1	0.02
Herrington	2746	6.3	0.02
Herrington	2747	6.3	0.02
Herrington	2748	6.3	0.02
Herrington	2749	6.3	0.02
Herrington	2750	6.2	0.03

Herrington (1) Av K = 0.305 md

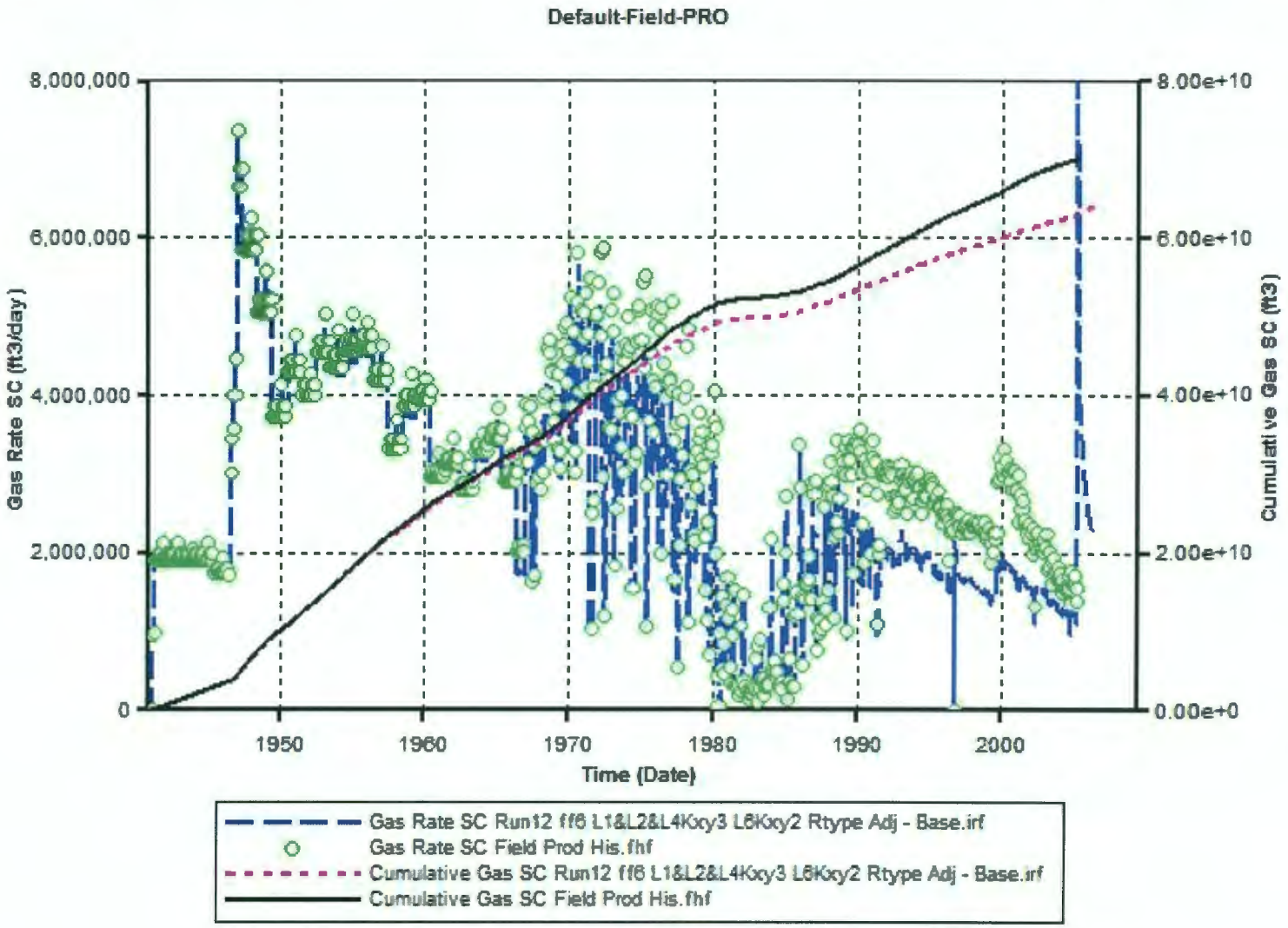
Perm can be multiplied by 3 (over starting multipier)

Figure 34



Sim 11: L1, L2, and L4 Kxy*3 (over starting multiplier)

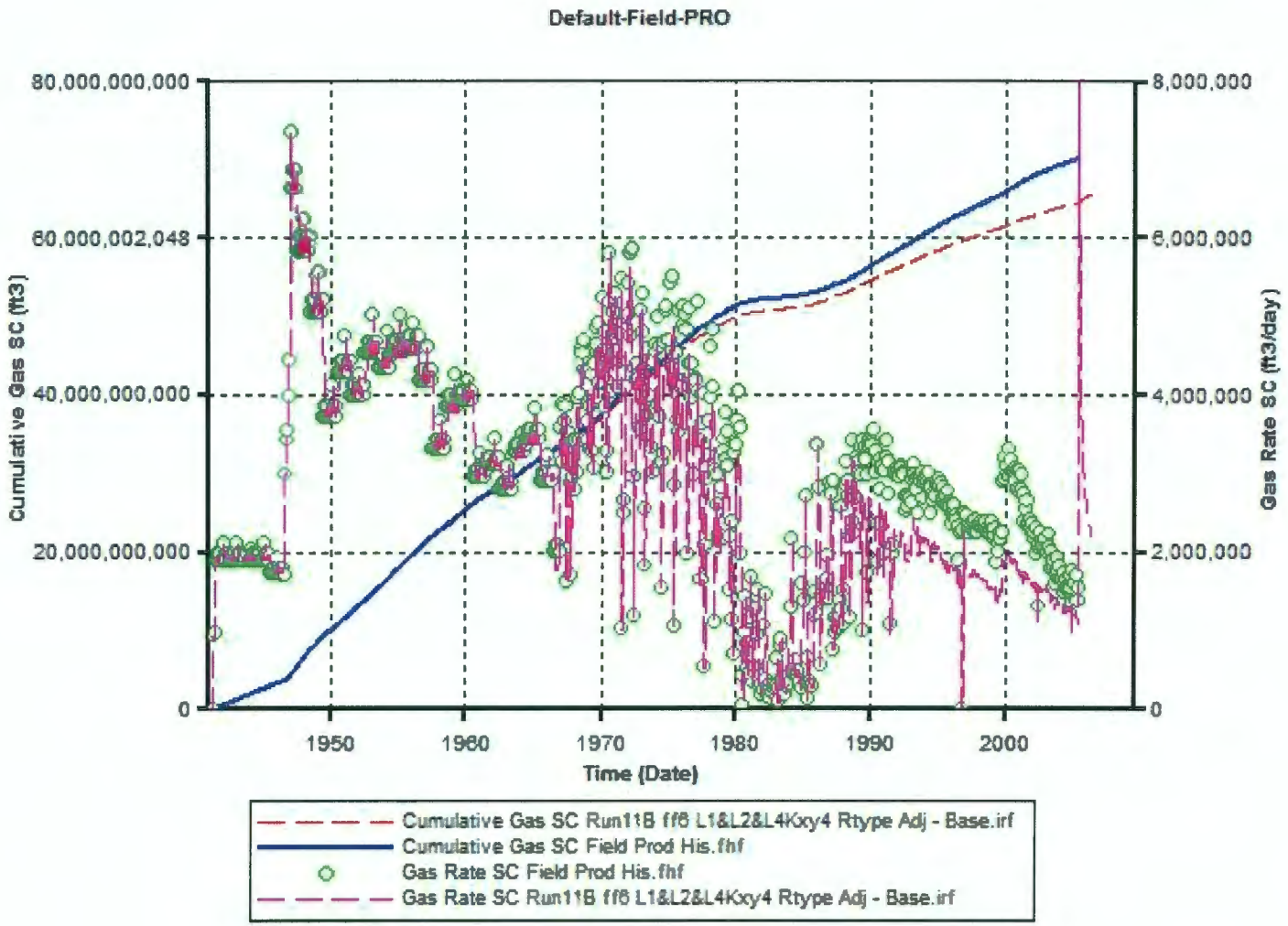
Figure 35



Sim 12: L1, L2, and L4 Kxy*3, L6 Kxy*2

Field cum pre-1970 almost matched in both cases

Figure 36



Sim 11B: L1, L2, and L4 Kxy*4 (over starting multiplier)

Field prod match obtained pre-1970

Figure 37

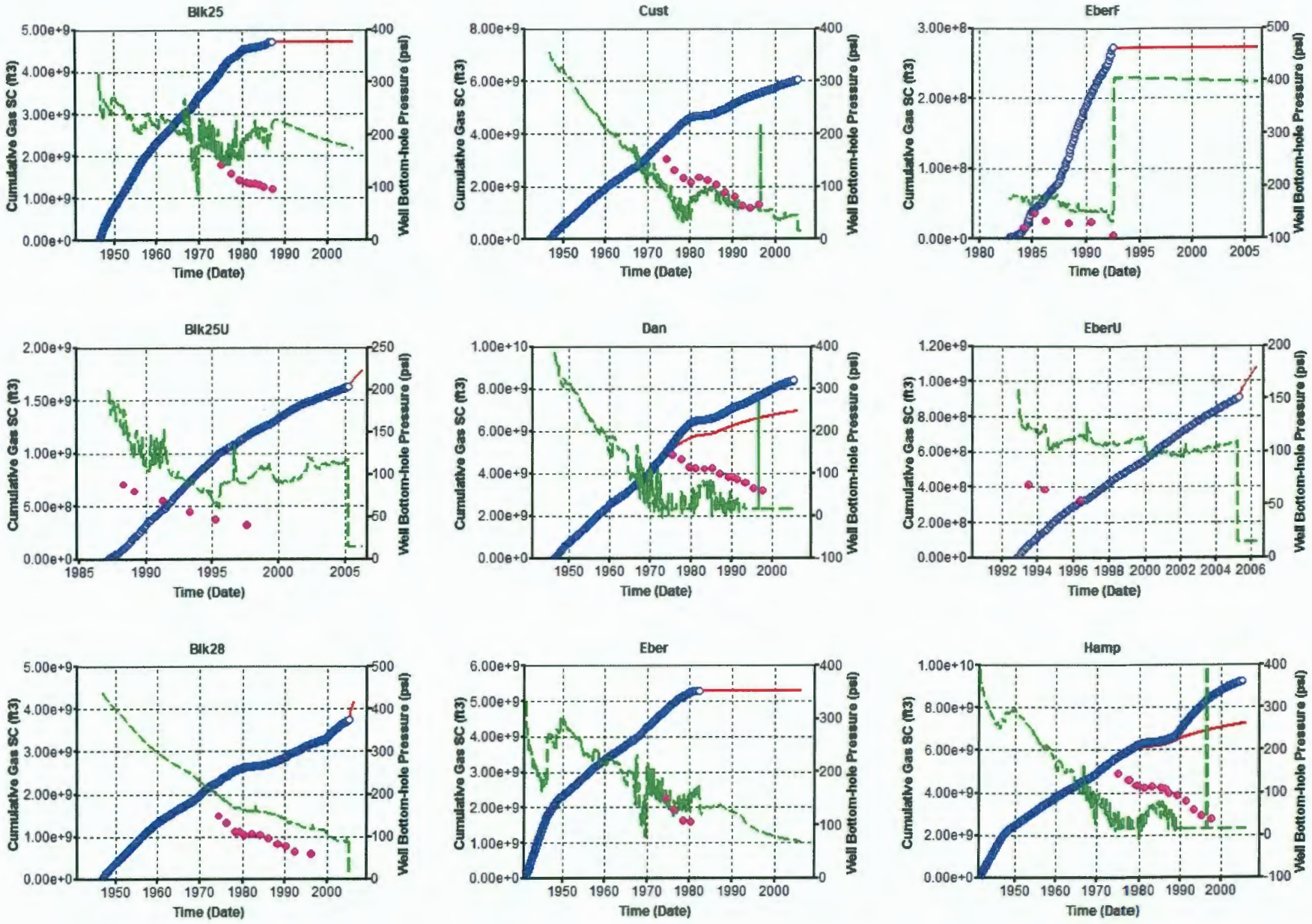
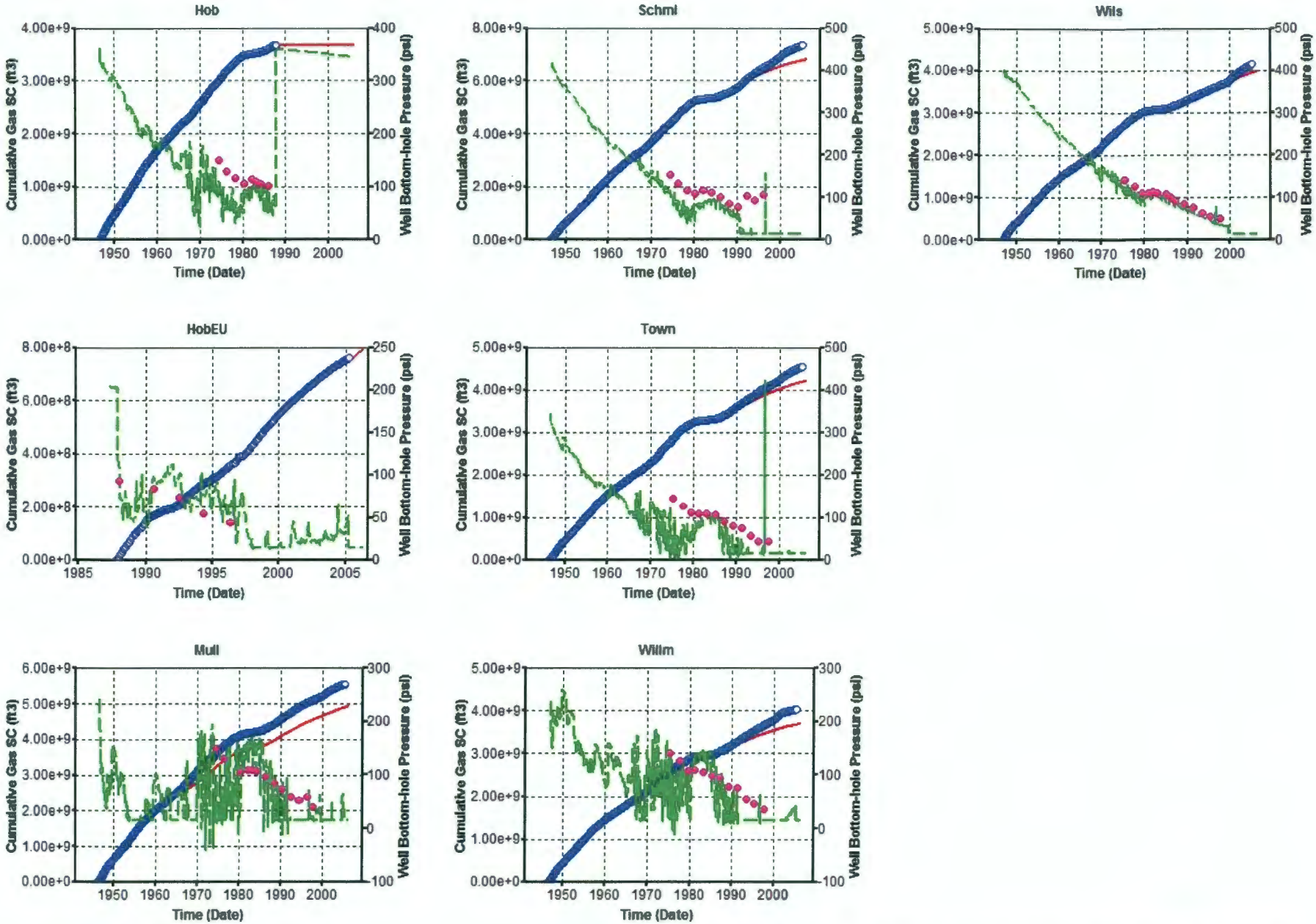


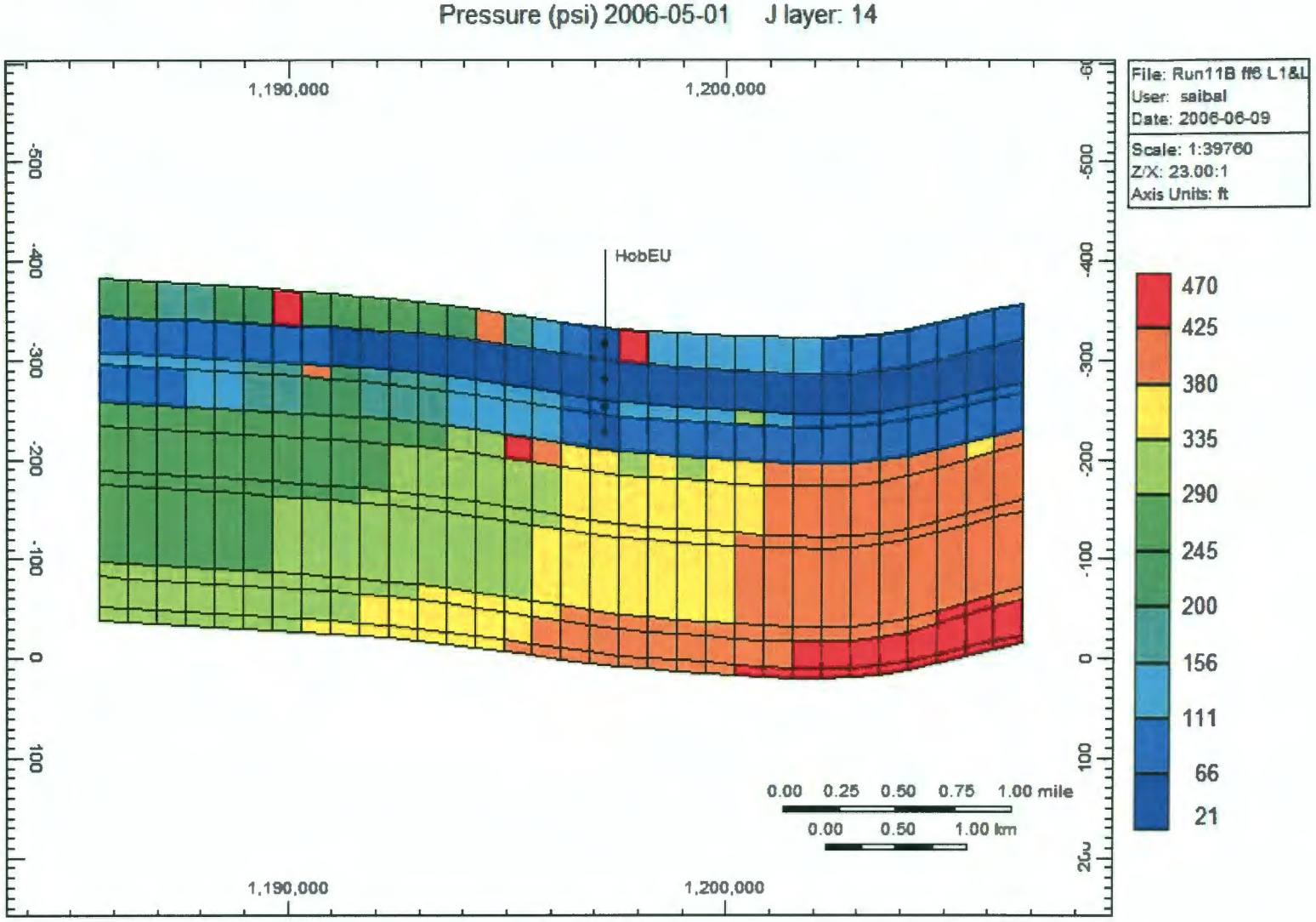
Figure 38

Sim 11B: L1, L2, and L4 Kxy*4 (over starting multiplier)



Sim 11B: L1, L2, and L4 Kxy*4 (over starting multiplier)

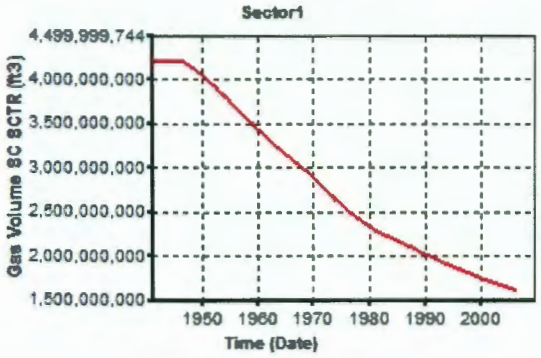
Figure 39

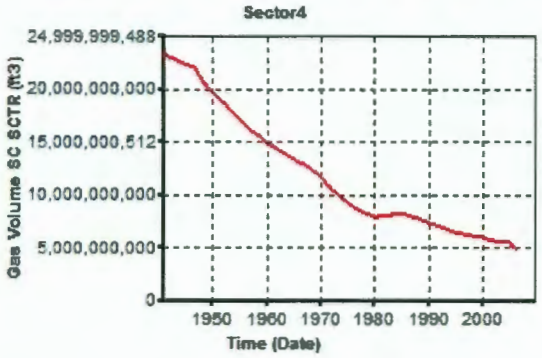


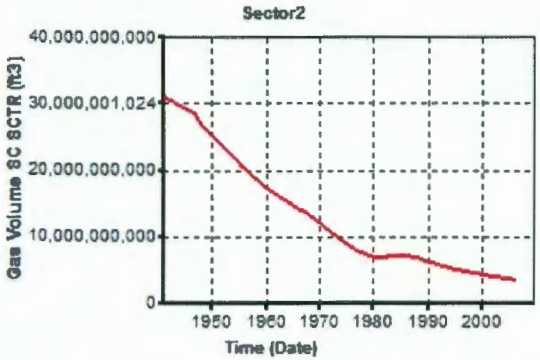
Sim 11B: L1, L2, and L4 Kxy*4 (over starting multiplier)

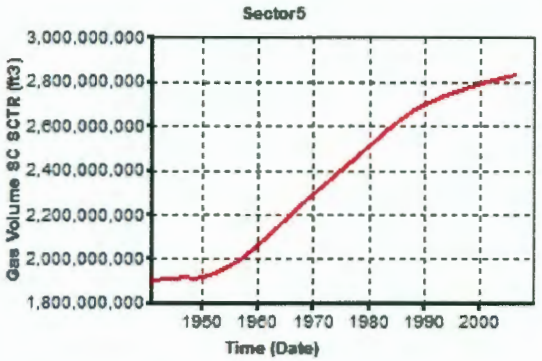
Figure 40

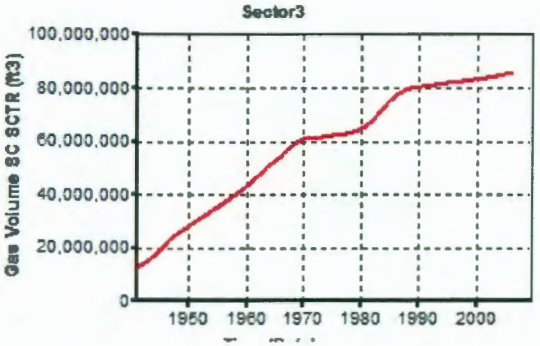
Run11B ff6 L1&L2&L4Kxy4 Rtype Adj - Base.irf

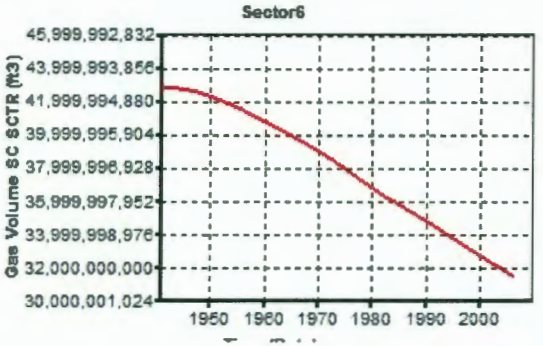












		OGIP in top 4 layers, bcf	58.1
Layer	Name	Marty's OGIP	Sim OGIP
1	Hrngtn	4	4.2
2	Krider	31	30.8
3	Odell	0	0.0123
4	Winf	23	23.1
5	Gage	2	1.89
6	Twnd	42	42.85
7	B/Twnd	3	3.04
8	Ftrly	23	25.19
9	Matfield	0	0
10	Wreford	0	0.0097
11	A1_ SH	0	0
At 450 psi, bcf OGIP		128	131.1

Sim 11B: L1, L2, and L4 Kxy*4 (over starting multiplier)

Figure 41

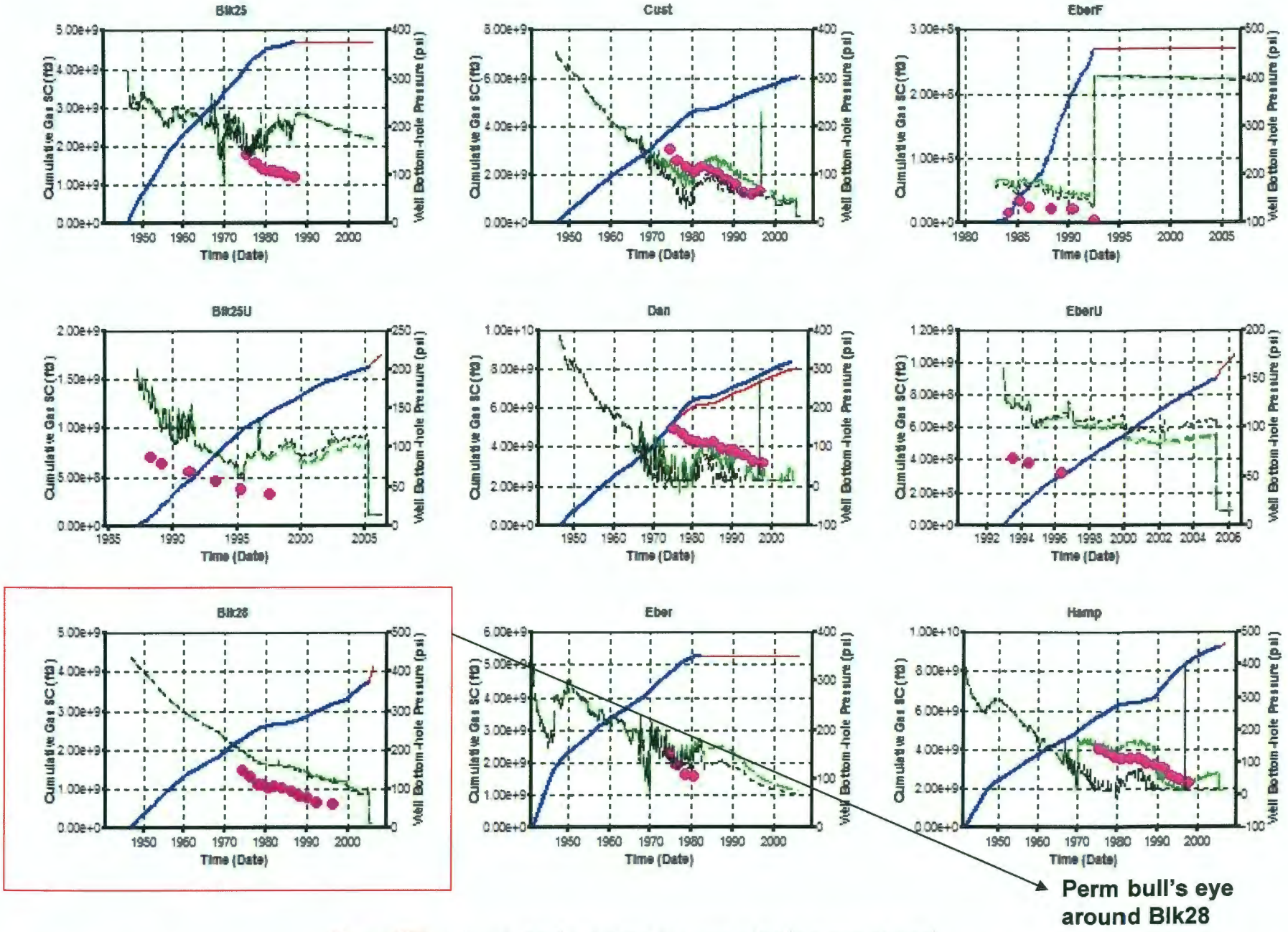
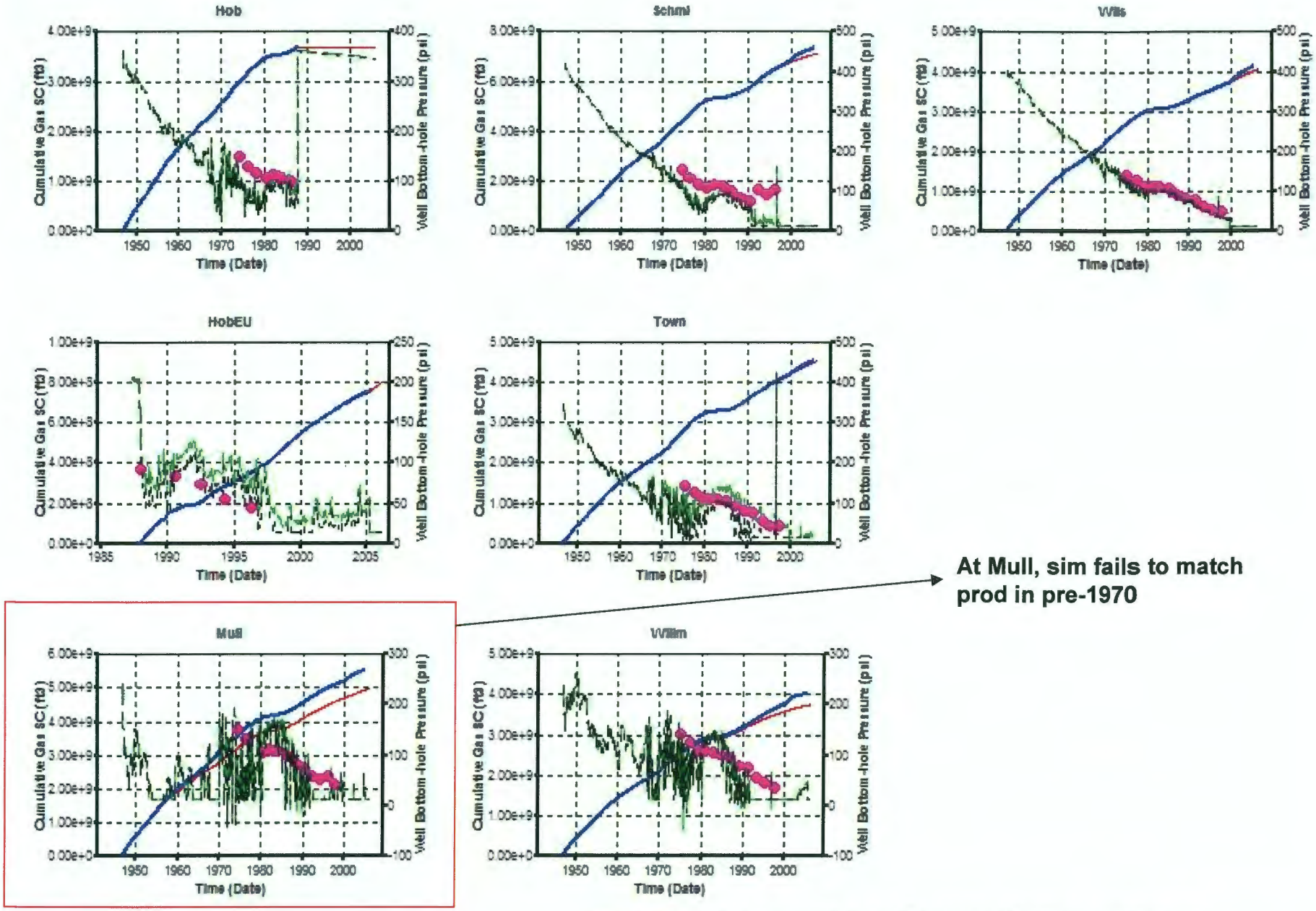


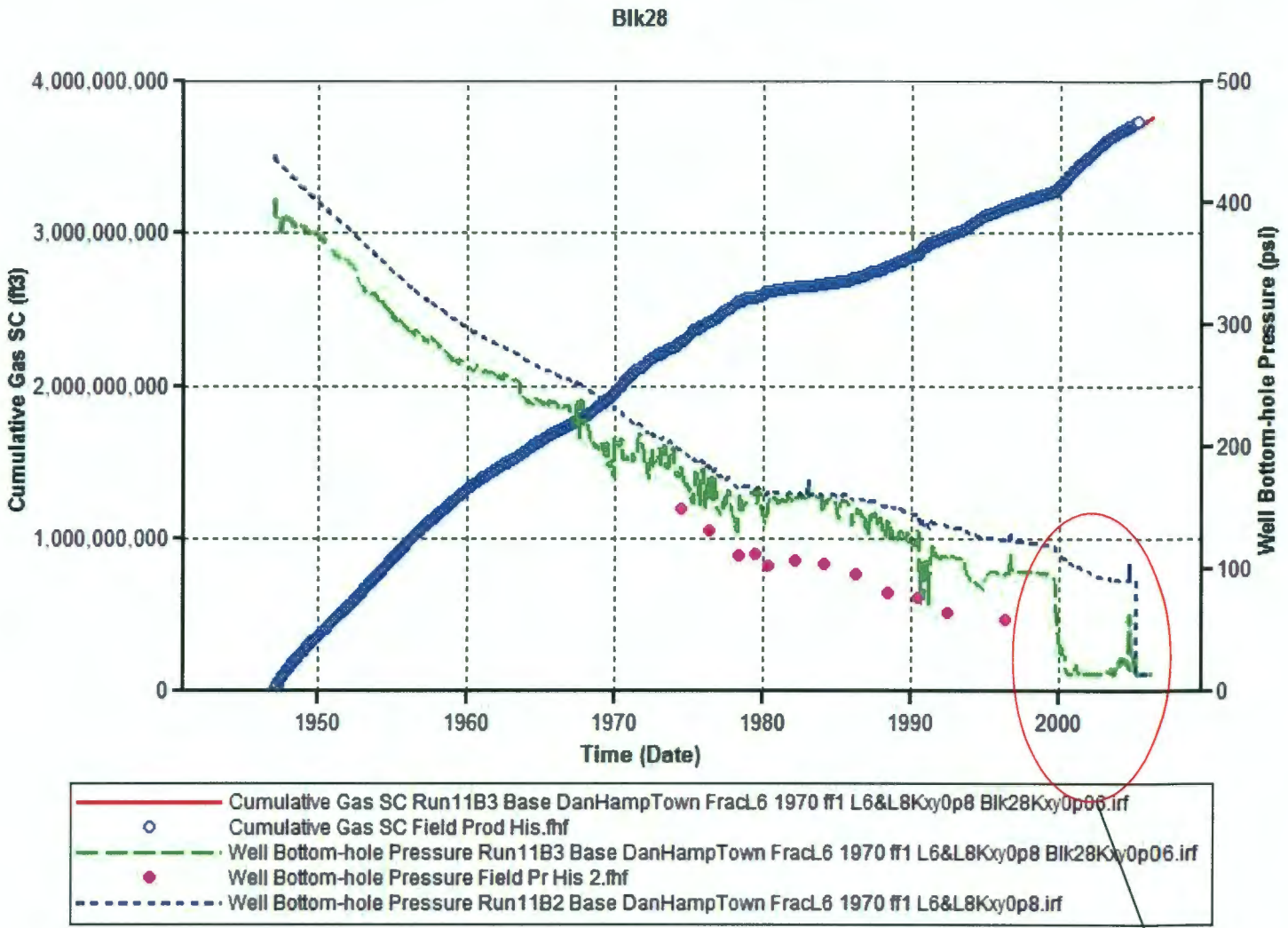
Figure 42

Sim 11B2: L1, L2, and L4 Kxy*4 (over starting multiplier)
Dan, Hamp, and Town – post 1970, Frac L6, ff = 1, Kxy L6 & L8 *0.8
Black – Run 11B Pwf. Green – Run 11B2 Pwf



Sim 11B2: L1, L2, and L4 Kxy*4 (over starting multiplier)
Dan, Hamp, and Town – post 1970, Frac L6, ff = 1, Kxy L6 & L8 *0.8
Black – Run 11B Pwf. Green – Run 11B2 Pwf

Figure 43



Sim 11B3: L1, L2, and L4 Kxy*4 (over starting multiplier)

Dan, Hamp, and Town – post 1970, Frac L6, ff = 1, Kxy L6 & L8 *0.8

Blk28 – L4 Lxy*0.06 (bring Kxy close to that in other wells in L4)

Matches at other wells remain unchanged from Run 11B2

Pwf = 14.7 psi to meet prod

Figure 44

A.

Model	Formation	Core Kxy (mean)	Model Kxy	Model Kz	Multiplier
1	Herrington	0.286	0.0274	0.000005	10.4
2	Krider	2.246	1.7833	0.036	1.3
3	Odell	0.067	0.0005	0.000007	134.0
4	Winfield	3.348	2.2702	0.00138	1.5
5	Gage	0.359	0.0077	0.0016	46.6
6	Towanda	0.928	1.126	0.0586	0.8
7	B/TWND	0.3	0.0385	0.00323	7.8
8	Ft. Riley	0.215	0.2929	0.0273	0.7
9	Matfield	1.518	0.0032	0.00068	474.4
10	Wreford	0.315	1.21	0.027	0.3
11	A1-SH		0.0029	0.0011	

B.

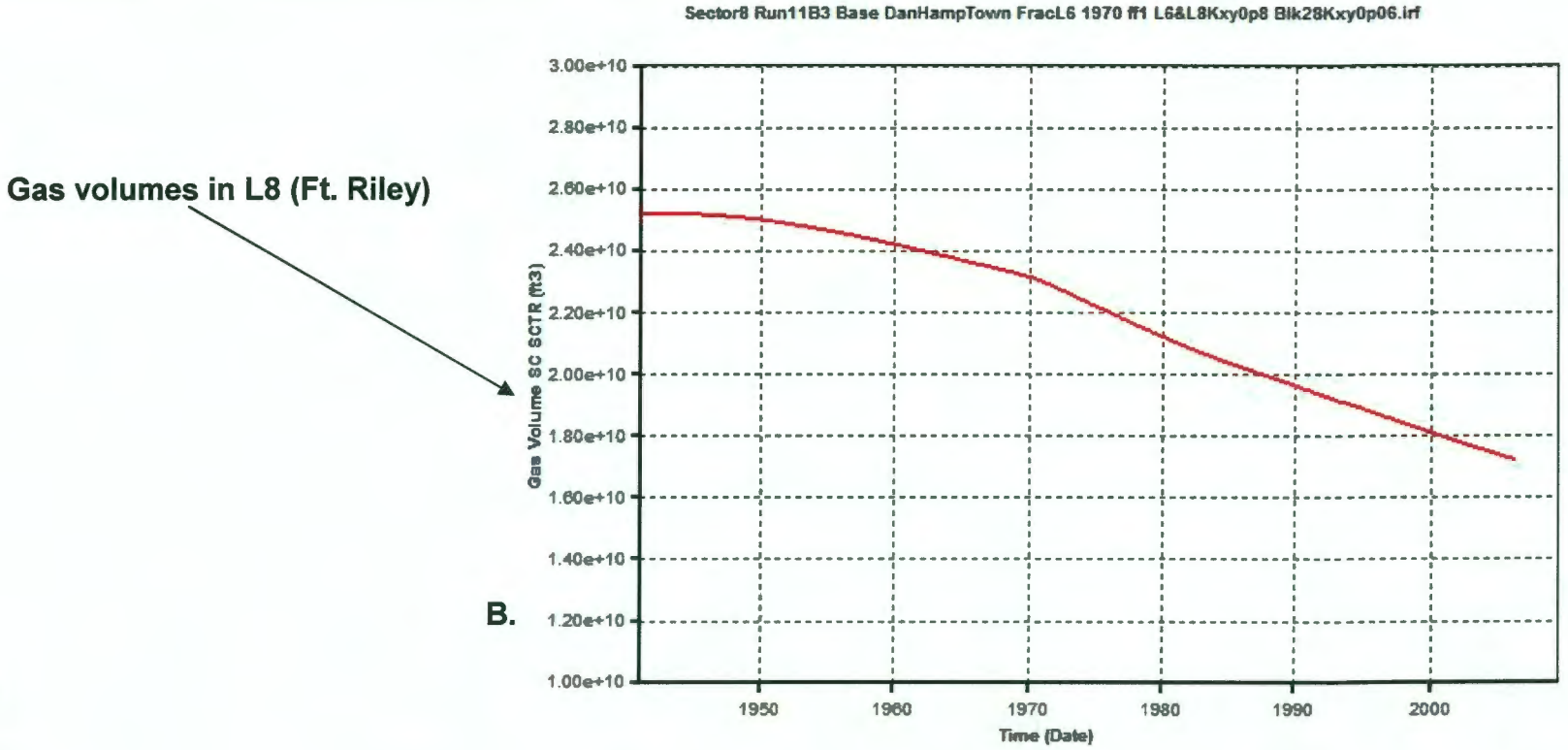
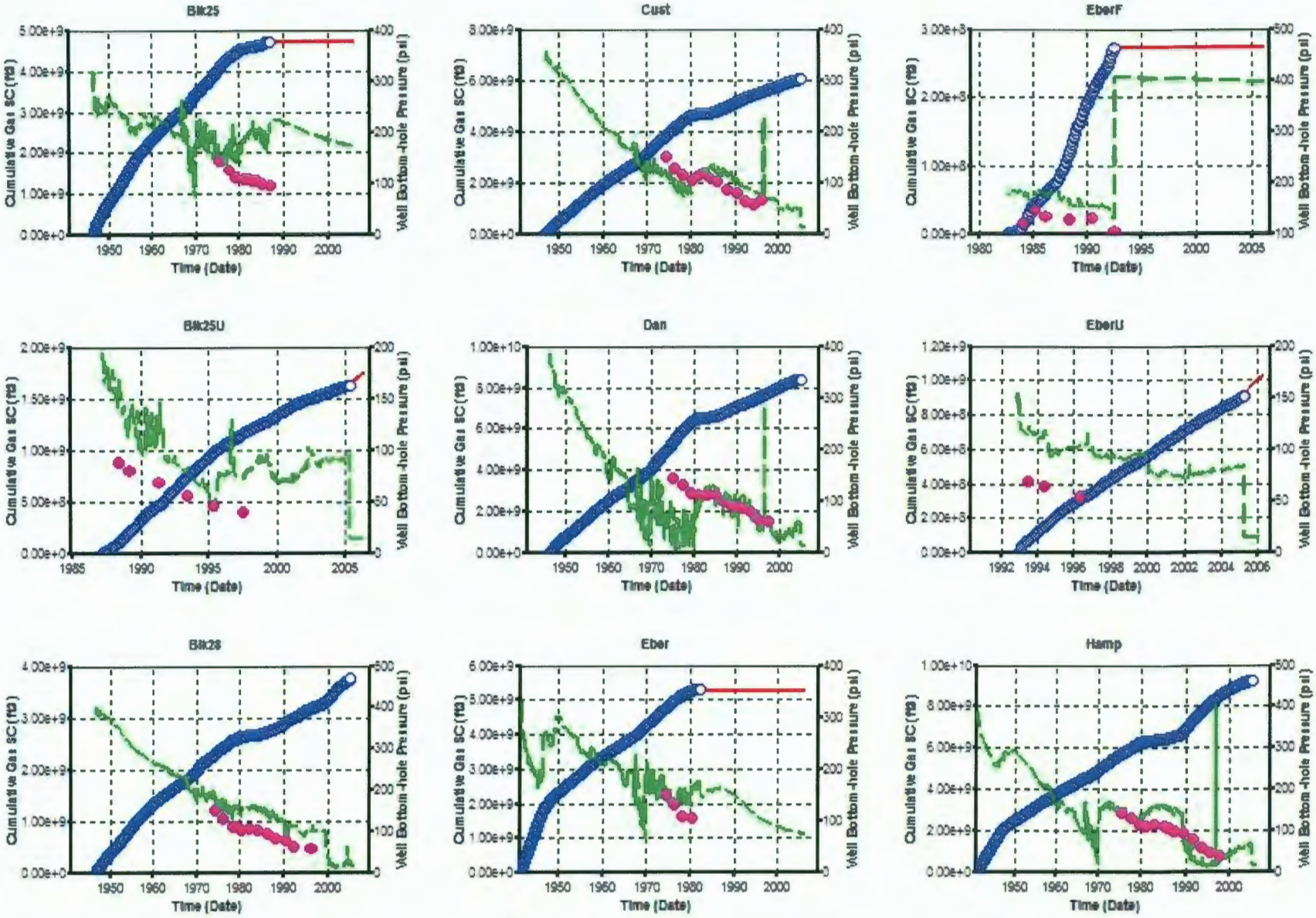


Figure 45



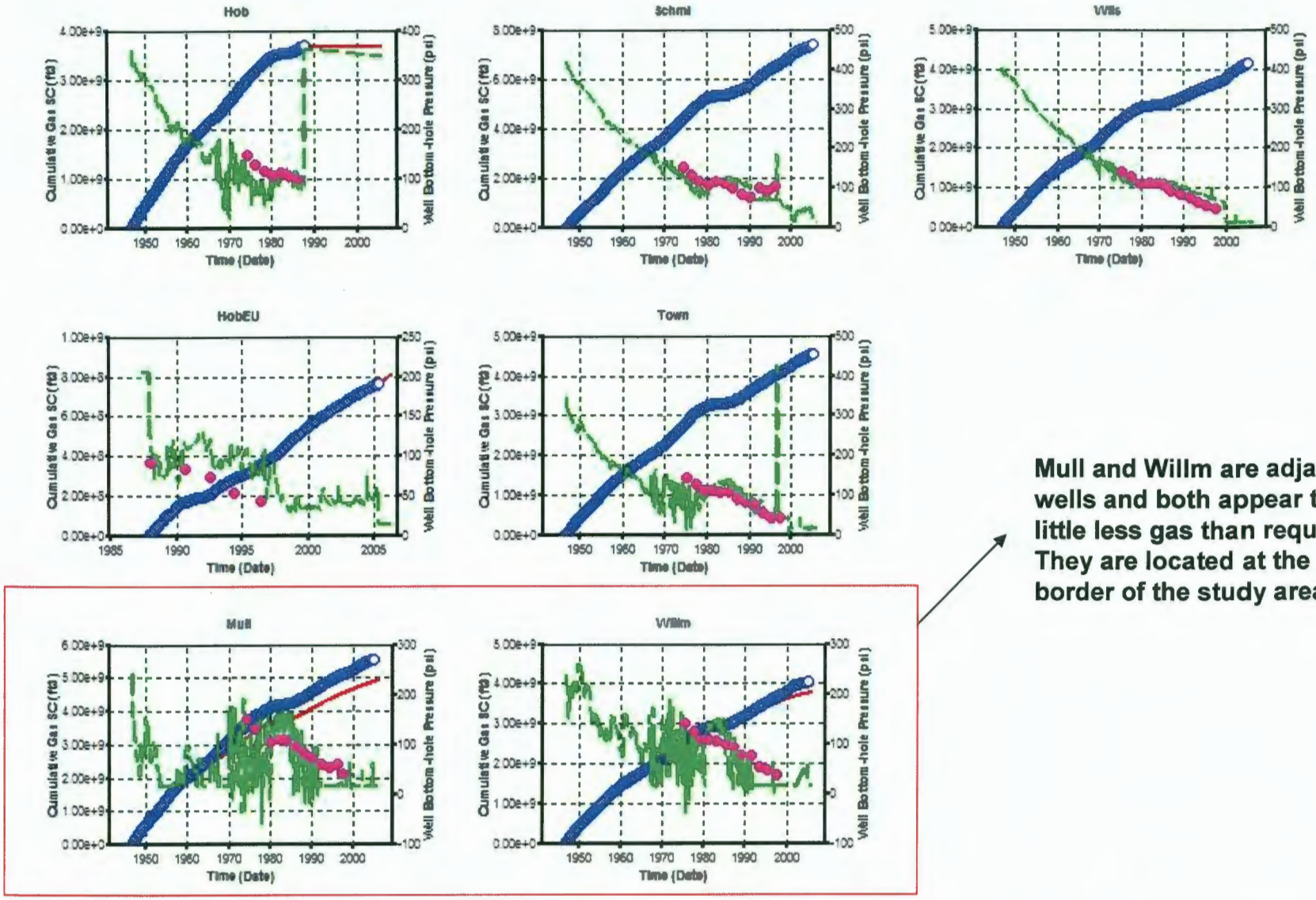
Sim 11B6: L1, L2, and L4 Kxy*4 (over starting multiplier)

Dan, Hamp, and Town – post 1970, Frac L6, ff = 1, Kxy L6 & L8 *0.8

Blk28 – L4 Lxy*0.06 (bring Kxy close to that in other wells in L4)

Dan ff=4 post 1970, Schm fracL6 post 1970 ff =1, L7 Kz*0.1

Figure 46



Mull and Willm are adjacent wells and both appear to have a little less gas than required. They are located at the southern border of the study area.

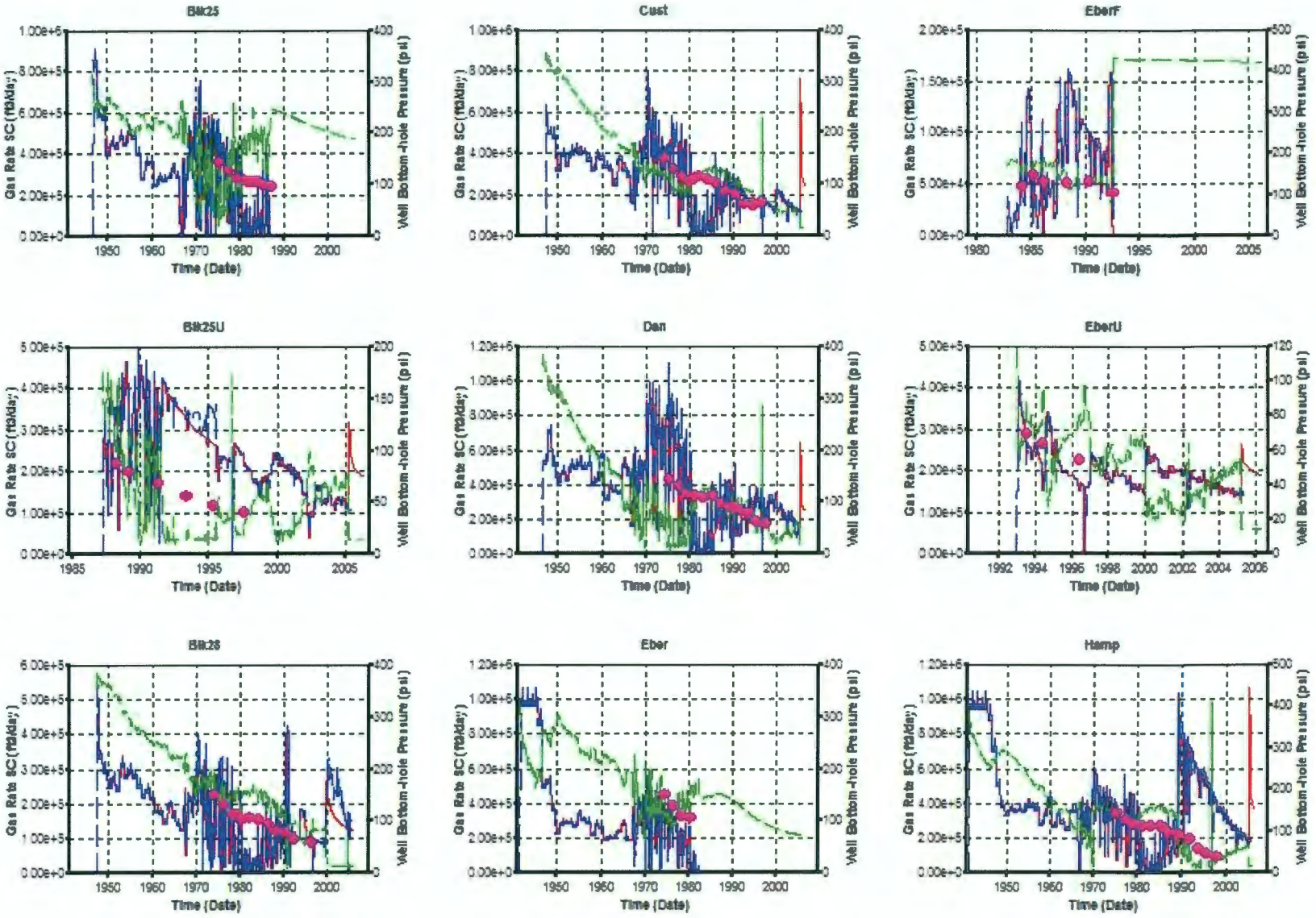
Sim 11B6: L1, L2, and L4 Kxy*4 (over starting multiplier)

Dan, Hamp, and Town – post 1970, Frac L6, ff = 1, Kxy L6 & L8 *0.8

Blk28 – L4 Lxy*0.06 (bring Kxy close to that in other wells in L4)

Dan ff=4 post 1970, Schm fracL6 post 1970 ff =1, L7 Kz*0.1

Figure 47

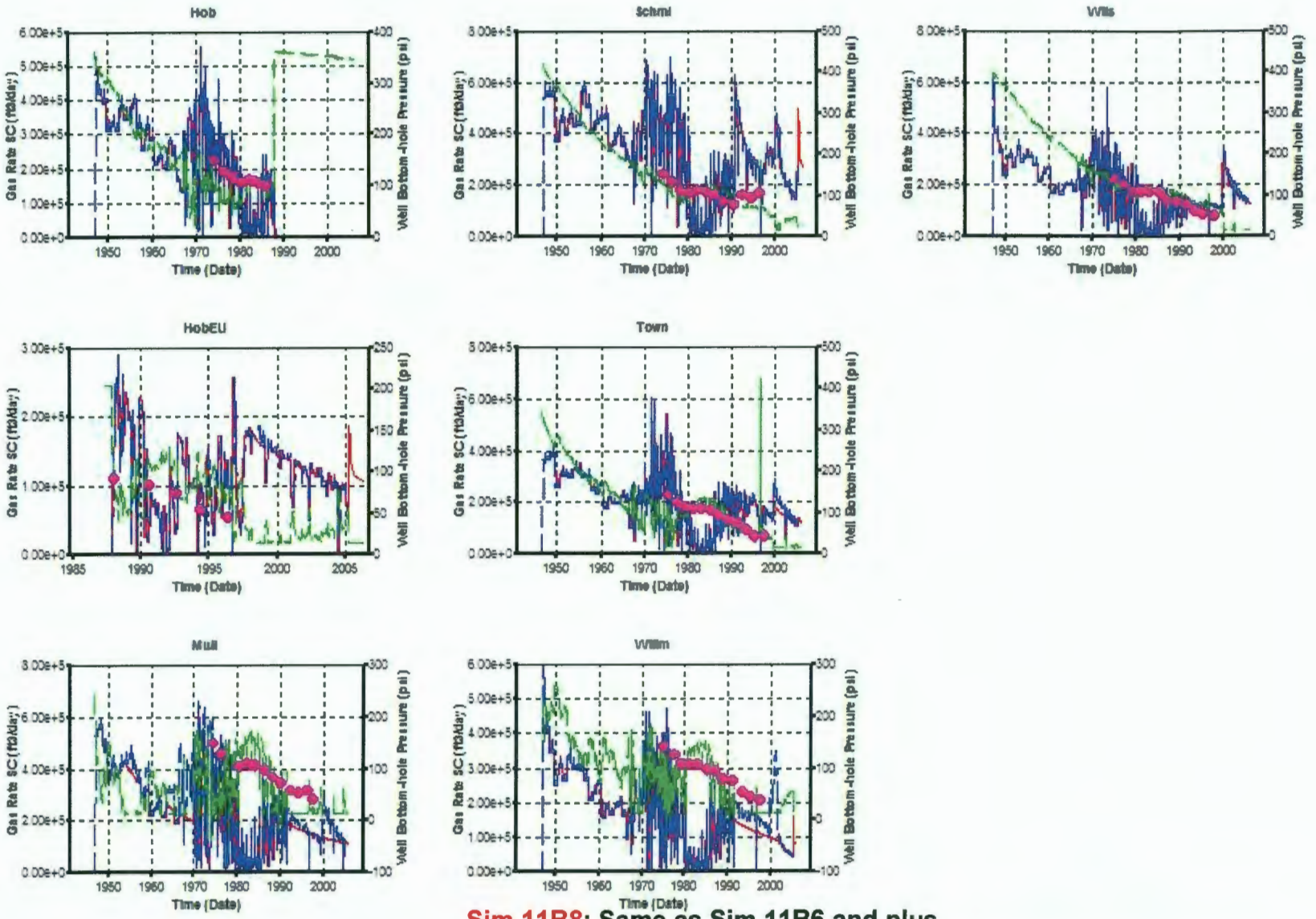


Sim 11B8: Same as Sim 11B6 and plus

Blk28 L4 Kxy*0.67 ff=3, Blk25 & 25U ff = 1, Eber ff = 2, EberF & U ff = 2

HobEU ff=3

Figure 48



Sim 11B8: Same as Sim 11B6 and plus

Blk28 L4 Kxy*0.67 ff=3, Blk25 & 25U ff = 1, Eber ff = 2, EberF & U ff = 2

HobEU ff=3

Figure 49

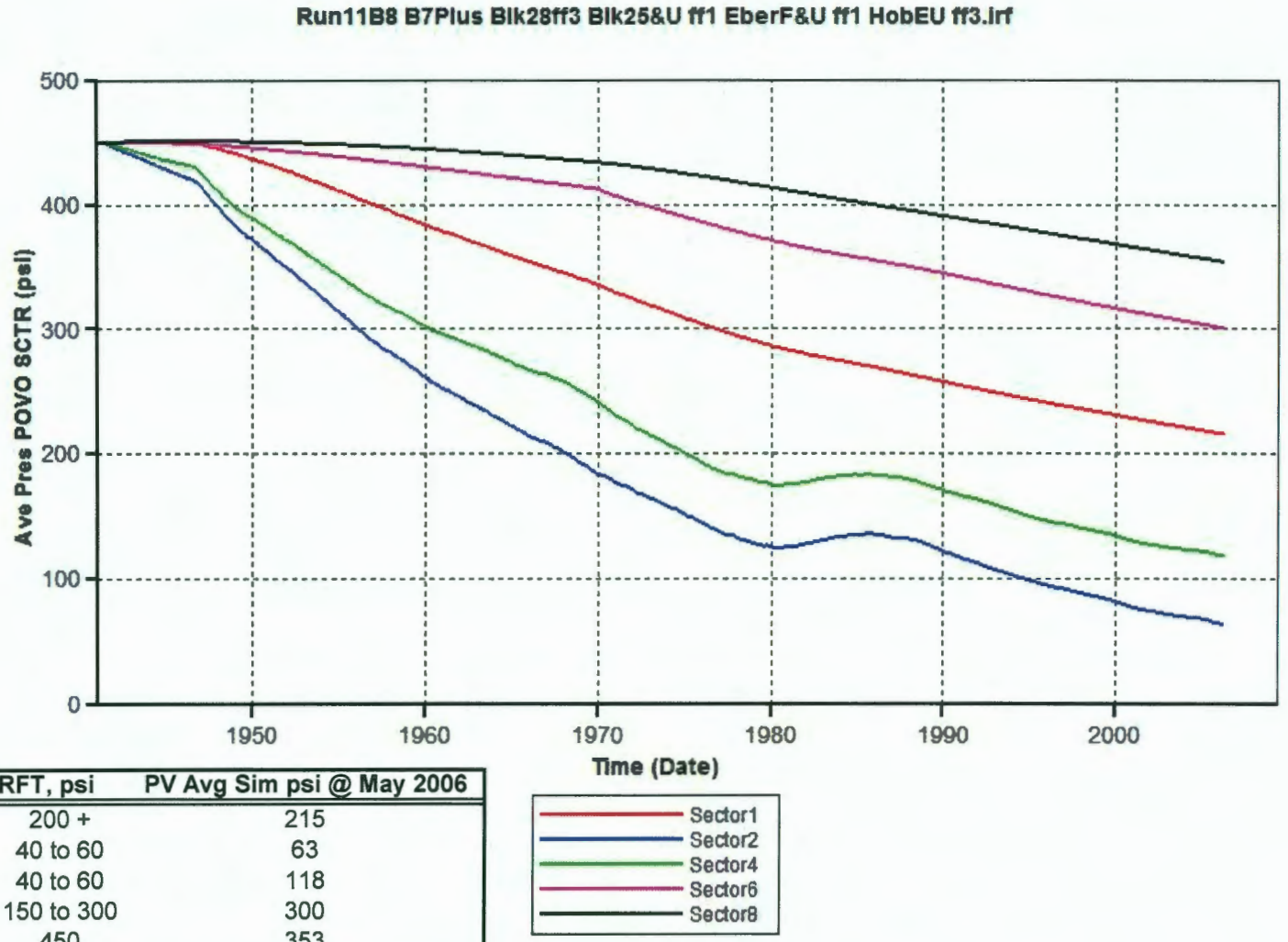
Well	Production match	Flowing Pressure match	Production spike when freed of flow constraints
Blackmer 25	Yes	BHFP>WHFP - midway	Shut-in
Blackmer 25U	Yes	Close - but low	Yes
Blackmer 28	Yes	BHFP>WHFP	No - unable to match prod from 2000
Custer	Yes	Yes	Yes
Daniels	Yes	Yes	Yes
Ebersole	Yes	Close	Shut-in
Ebersole F	Yes	Close	Shut-in
Ebersole U	Yes	Close	Yes - small
Hampston	Yes	Close	Yes
Hobbler	Yes	Close	Shut-in
HobbE	Yes	Close	Yes - small
Muller	Short initally & at end		
Schmelzel	Yes	Close	Yes
Towner	Yes	Yes	No
Willams	Short at end		
Wilson	Yes	Yes	No

Sim 11B8: Same as Sim 11B6 and plus

Blk28 L4 Kxy*0.67 ff=3, Blk25 & 25U ff = 1, Eber ff = 2, EberF & U ff = 2

HobEU ff=3

Figure 50



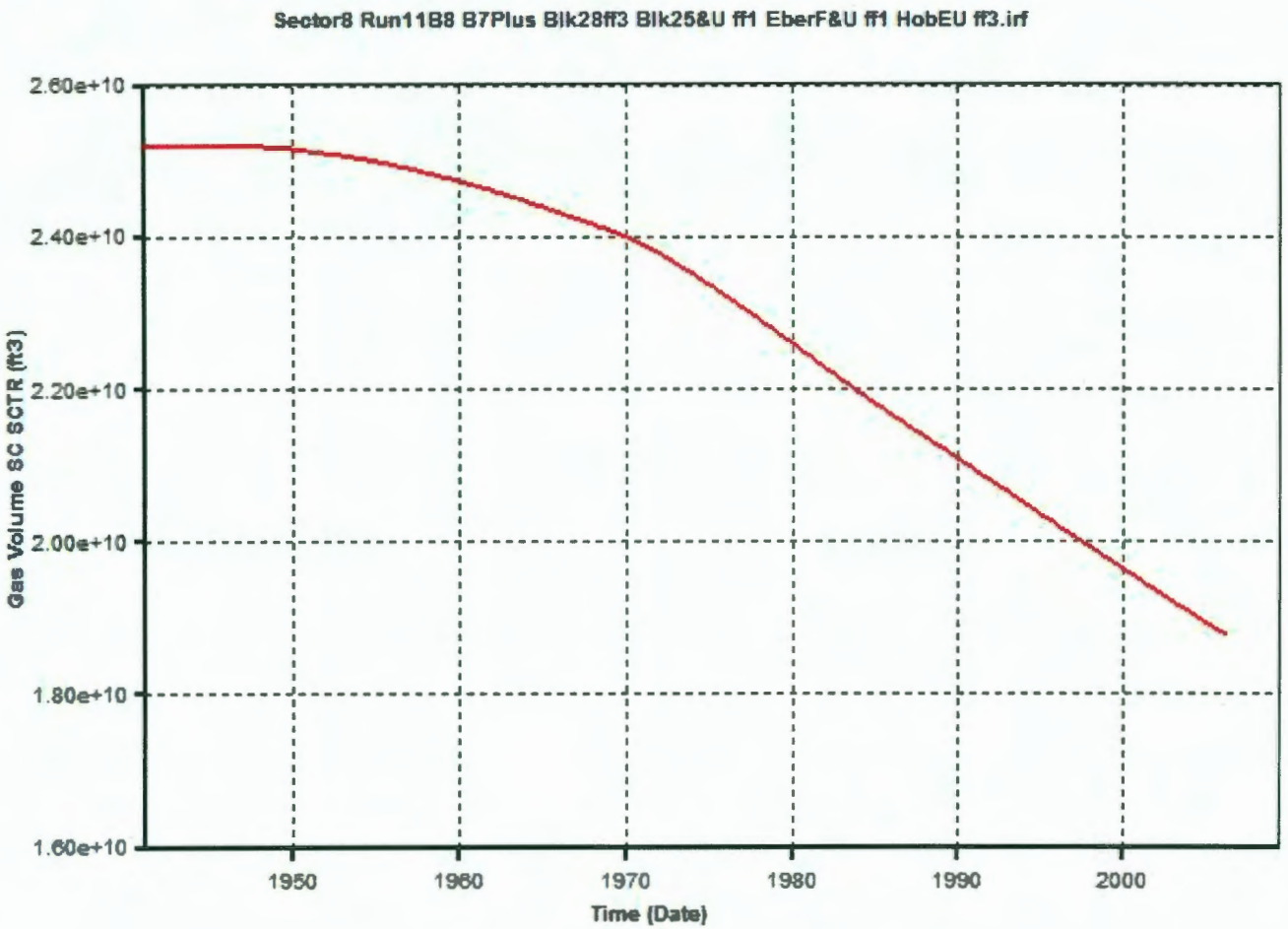
	RFT, psi	PV Avg Sim psi @ May 2006
Herrington	200 +	215
Krider	40 to 60	63
Winfield	40 to 60	118
Towanda	150 to 300	300
Ft. Riley	450	353

Sim 11B8: Same as Sim 11B6 and plus

Blk28 L4 Kxy*0.67 ff=3, Blk25 & 25U ff = 1, Eber ff = 2, EberF & U ff = 2

HobEU ff=3

Figure 51



Sim 11B8: Same as Sim 11B6 and plus

Blk28 L4 Kxy*0.67 ff=3, Blk25 & 25U ff = 1, Eber ff = 2, EberF & U ff = 2

HobEU ff=3

Figure 52